Missouri University of Science and Technology
Scholars' Mine

Physics Faculty Research & Creative Works | Physics

01 Apr 2001

Electron Self-Energy for the K and L Shells at Low Nuclear Charge

Ulrich D. Jentschura
Missouri University of Science and Technology, ulj@mst.edu

Peter J. Mohr

Gerhard Soff

Follow this and additional works at: https://scholarsmine.mst.edu/phys_facwork

 Part of the Physics Commons

Recommended Citation

U. D. Jentschura et al., "Electron Self-Energy for the K and L Shells at Low Nuclear Charge," *Physical Review A. Atomic, Molecular, and Optical Physics*, vol. 63, no. 4, pp. 425121-425129, American Physical Society (APS), Apr 2001.
The definitive version is available at https://doi.org/10.1103/PhysRevA.63.042512

This Article - Journal is brought to you for free and open access by Scholars' Mine. It has been accepted for inclusion in Physics Faculty Research & Creative Works by an authorized administrator of Scholars' Mine. This work is protected by U. S. Copyright Law. Unauthorized use including reproduction for redistribution requires the permission of the copyright holder. For more information, please contact scholarsmine@mst.edu.

Electron self-energy for the *K* and *L* shells at low nuclear charge

Ulrich D. Jentschura,[1,2,*] Peter J. Mohr,[1,†] and Gerhard Soff[2,‡]
[1]*National Institute of Standards and Technology, Mail Stop 8401, Gaithersburg, Maryland 20899-8401*
[2]*Institut für Theoretische Physik, TU Dresden, Mommsenstraße 13, 01062 Dresden, Germany*
(Received 22 August 2000; published 21 March 2001)

A nonperturbative numerical evaluation of the one-photon electron self-energy for the *K*- and *L*-shell states of hydrogenlike ions with nuclear charge numbers $Z=1$ to 5 is described. Our calculation for the $1S_{1/2}$ state has a numerical uncertainty of 0.8 Hz in atomic hydrogen, and for the *L*-shell states ($2S_{1/2}$, $2P_{1/2}$, and $2P_{3/2}$) the numerical uncertainty is 1.0 Hz. The method of evaluation for the ground state and for the excited states is described in detail. The numerical results are compared to results based on known terms in the expansion of the self-energy in powers of $Z\alpha$.

DOI: 10.1103/PhysRevA.63.042512 PACS number(s): 31.30.Jv, 12.20.Ds, 06.20.Jr, 31.15.−p

I. INTRODUCTION

The nonperturbative numerical evaluation of radiative corrections to bound-state energy levels is interesting for two reasons. First, the recent dramatic increase in the accuracy of experiments that measure the transition frequencies in hydrogen and deuterium [1–3] necessitates a numerical evaluation (nonperturbative in the binding Coulomb field) of the radiative corrections to the spectrum of atomic systems with low nuclear charge *Z*. Second, the numerical calculation serves as an independent test of analytic evaluations which are based on an expansion in the binding field with an expansion parameter $Z\alpha$.

In order to address both issues, a high-precision numerical evaluation of the self energy of an electron in the ground state in hydrogenlike ions has been performed [4,5]. The approach outlined in [4] is generalized here to the *L* shell, and numerical results are obtained for the $(n=2)$ states $2S_{1/2}$, $2P_{1/2}$, and $2P_{3/2}$. Results are provided for atomic hydrogen, He^{+}, Li^{2+}, Be^{3+}, and B^{4+}.

It has been pointed out in [4,5] that the nonperturbative effects (in $Z\alpha$) can be large even for low nuclear charge and exceed the current experimental accuracy for atomic transitions. For example, the difference between the sum of the analytically evaluated terms up to the order of $\alpha(Z\alpha)^6$ and the final numerical result for the ground state is roughly 27 kHz for atomic hydrogen and about 3200 kHz for He^{+}. For the $2S$ state the difference is 3.5 kHz for atomic hydrogen and 412 kHz for He^{+}. The large difference between the result obtained by an expansion in $Z\alpha$ persists even after the inclusion of a result recently obtained in [6] for the logarithmic term of order $\alpha(Z\alpha)^7\ln(Z\alpha)^{-2}$. For the ground state, the difference between the all-order numerical result and the sum of the perturbative terms is still 13 kHz for atomic hydrogen and 1600 kHz for He^{+}. For the $2S$ state, the difference amounts to 1.6 kHz for atomic hydrogen and to 213 kHz for He^{+}.

These figures should be compared to the current experimental precision. The most accurately measured transition to date is the $1S$-$2S$ frequency in hydrogen; it has been measured with a relative uncertainty of 1.8 parts in 10^{14} or 46 Hz [3]. This experimental progress is due in part to the use of frequency chains that bridge the range between optical frequencies and the microwave cesium time standard. The uncertainty of the measurement is likely to be reduced by an order of magnitude in the near future [3,7]. With trapped hydrogen atoms, it should be feasible to observe the $1S$-$2S$ frequency with an experimental linewidth that approaches the 1.3 Hz natural width of the $2S$ level [8,9].

The perturbation series in $Z\alpha$ is slowly convergent. The all-order numerical calculation presented in this paper essentially eliminates the uncertainty from unevaluated higher-order analytic terms, and we obtain results for the self-energy remainder function $G_{\rm SE}$ with a precision of roughly 0.8 $\times Z^4$ Hz for the ground state of atomic hydrogen and 1.0 $\times Z^4$ Hz for the $2S$ state.

In the evaluation, we take advantage of resummation and convergence acceleration techniques. The resummation techniques provide an efficient method of evaluation of the Dirac-Coulomb Green function to a relative uncertainty of 10^{-24} over a wide parameter range [5]. The convergence acceleration techniques remove the principal numerical difficulties associated with the singularity of the relativistic propagators for nearly equal radial arguments [10].

The one-photon self-energy treated in the current investigation is about two orders of magnitude larger than the other contributions to the Lamb shift in atomic hydrogen. A comprehensive review of the various contributions to the Lamb shift in hydrogenlike atoms in the full range of nuclear charge numbers $Z=1$–110 has been given in [11–14].

This paper is organized as follows. The method of evaluation is discussed in Sec. II. The calculation is divided into a low-energy part and a high-energy contribution. The low-energy part is treated in Sec. III, and the high-energy part is discussed in Sec. IV. Numerical results are compiled in Sec. V. Also in Sec. V, we compare numerical and analytic results for the Lamb shift in the region of low nuclear charge numbers. Of special importance is the consistency check with available analytic results [15,16] for higher-order bind-

*Electronic address: jentschura@physik.tu-dresden.de
†Electronic address: mohr@nist.gov
‡Electronic address: soff@physik.tu-dresden.de

 ©2001 The American Physical Society

ing corrections to the Lamb shift. We make concluding remarks in Sec. VI.

II. METHOD OF EVALUATION

A. Status of analytic calculations

The (real part of the) energy shift $\Delta E_{\rm SE}$ due to the electron self-energy radiative correction is usually written as

$$\Delta E_{\rm SE}=\frac{\alpha}{\pi}\frac{(Z\alpha)^4}{n^3}F(nl_j,Z\alpha)\,m_{\rm e}c^2, \tag{2.1}$$

where F is a dimensionless quantity. In the following, the natural unit system with $\hbar=c=m_{\rm e}=1$ and $e^2=4\pi\alpha$ is employed. Note that $F(nl_j,Z\alpha)$ is a dimensionless function which depends for a given atomic state with quantum numbers n, l, and j on only one argument (the coupling $Z\alpha$). For excited states, the (nonvanishing) imaginary part of the self-energy is proportional to the (spontaneous) decay width of the state. We will denote here the *real* part of the self-energy by $\Delta E_{\rm SE}$, exclusively. The semianalytic expansion of $F(nl_j,Z\alpha)$ about $Z\alpha=0$ for a general atomic state with quantum numbers n, l, and j gives rise to the semianalytic expansion,

$$\begin{aligned}F(nl_j,Z\alpha)=&A_{41}(nl_j)\ln(Z\alpha)^{-2}+A_{40}(nl_j)+(Z\alpha)A_{50}(nl_j)\\&+(Z\alpha)^2[A_{62}(nl_j)\ln^2(Z\alpha)^{-2}+A_{61}(nl_j)\\&\times\ln(Z\alpha)^{-2}+G_{\rm SE}(nl_j,Z\alpha)].\end{aligned} \tag{2.2}$$

For particular states, some of the coefficients may vanish. Notably, this is the case for P states, which are less singular than S states at the origin [see Eq. (2.4) below]. For the $nS_{1/2}$ state ($l=0,j=1/2$), none of the terms in Eq. (2.2) vanishes, and we have

$$\begin{aligned}F(nS_{1/2},Z\alpha)=&A_{41}(nS_{1/2})\ln(Z\alpha)^{-2}+A_{40}(nS_{1/2})\\&+(Z\alpha)A_{50}(nS_{1/2})+(Z\alpha)^2\\&\times[A_{62}(nS_{1/2})\ln^2(Z\alpha)^{-2}+A_{61}(nS_{1/2})\\&\times\ln(Z\alpha)^{-2}+G_{\rm SE}(nS_{1/2},Z\alpha)].\end{aligned} \tag{2.3}$$

The A coefficients have two indices, the first of which denotes the power of $Z\alpha$ [including those powers explicitly shown in Eq. (2.1)], while the second index denotes the power of the logarithm $\ln(Z\alpha)^{-2}$. For P states, the coefficients A_{41}, A_{50}, and A_{62} vanish, and we have

$$\begin{aligned}F(nP_j,Z\alpha)=&A_{40}(nP_j)+(Z\alpha)^2[A_{61}(nP_j)\\&\times\ln(Z\alpha)^{-2}+G_{\rm SE}(nP_j,Z\alpha)].\end{aligned} \tag{2.4}$$

For S states, the self-energy remainder function $G_{\rm SE}$ can be expanded semianalytically as

$$\begin{aligned}G_{\rm SE}(nS_{1/2},Z\alpha)=&A_{60}(nS_{1/2})+(Z\alpha)[A_{71}(nS_{1/2})\ln(Z\alpha)^{-2}\\&+A_{70}(nS_{1/2})+o(Z\alpha)]\end{aligned} \tag{2.5}$$

(for the ''order'' symbols o and O we follow the usual convention, see, e.g., [17,18]). For P states, the semianalytic expansion of $G_{\rm SE}$ reads

$$G_{\rm SE}(nP_j,Z\alpha)=A_{60}(nP_j)+(Z\alpha)[A_{70}(nP_j)+o(Z\alpha)]. \tag{2.6}$$

The fact that $A_{71}(nP_j)$ vanishes has been pointed out in [6]. We list below the analytic coefficients and the Bethe logarithms relevant to the atomic states under investigation. For the ground state, the coefficients A_{41} and A_{40} were obtained in [19–25], the correction term A_{50} was found in [26–28], and the higher-order binding corrections A_{62} and A_{61} were evaluated in [29–37,15]. The results are

$$\begin{aligned}A_{41}(1S_{1/2})&=\tfrac{4}{3},\\A_{40}(1S_{1/2})&=\tfrac{10}{9}-\tfrac{4}{3}\ln k_0(1S),\\A_{50}(1S_{1/2})&=4\pi\left[\tfrac{139}{128}-\tfrac{1}{2}\ln 2\right],\\A_{62}(1S_{1/2})&=-1,\\A_{61}(1S_{1/2})&=\tfrac{28}{3}\ln 2-\tfrac{21}{20}.\end{aligned} \tag{2.7}$$

The Bethe logarithm $\ln k_0(1S)$ has been evaluated in [38] and [39–43] as

$$\ln k_0(1S)=2.984\,128\,555\,8(3). \tag{2.8}$$

For the $2S$ state, we have

$$\begin{aligned}A_{41}(2S_{1/2})&=\tfrac{4}{3},\\A_{40}(2S_{1/2})&=\tfrac{10}{9}-\tfrac{4}{3}\ln k_0(2S),\\A_{50}(2S_{1/2})&=4\pi\left[\tfrac{139}{128}-\tfrac{1}{2}\ln 2\right],\\A_{62}(2S_{1/2})&=-1,\\A_{61}(2S_{1/2})&=\tfrac{16}{3}\ln 2+\tfrac{67}{30}.\end{aligned} \tag{2.9}$$

The Bethe logarithm $\ln k_0(2S)$ has been evaluated (see [38–43], the results exhibit varying accuracy) as

$$\ln k_0(2S)=2.811\,769\,893(3). \tag{2.10}$$

It might be worth noting that the value for $\ln k_0(2S)$ given in [44] evidently contains a typographical error. Our independent reevaluation confirms the result given in Eq. (2.10), which was originally obtained in [38] to the required precision. For the $2P_{1/2}$ state we have

$$\begin{aligned}A_{40}(2P_{1/2})&=-\tfrac{1}{6}-\tfrac{4}{3}\ln k_0(2P),\\A_{61}(2P_{1/2})&=\tfrac{103}{180}.\end{aligned} \tag{2.11}$$

Note that a general analytic result for the logarithmic correction A_{61} as a function of the bound-state quantum numbers n, l, and j can be inferred from Eq. (4.4a) of [34,35] upon subtraction of the vacuum polarization contribution implic-

itly contained in the quoted equation. The Bethe logarithm for the $2P$ states reads [38,45]

$$\ln k_0(2P) = -0.030\,016\,708\,9(3). \tag{2.12}$$

Because the Bethe logarithm is an inherently nonrelativistic quantity, it is spin-independent and therefore independent of the total angular momentum j for a given orbital angular momentum l. For the $2P_{3/2}$ state the analytic coefficients are

$$A_{40}(2P_{3/2}) = \tfrac{1}{12} - \tfrac{4}{3}\ln k_0(2P),$$
$$A_{61}(2P_{3/2}) = \tfrac{29}{90}. \tag{2.13}$$

We now consider the limit of the function $G_{\rm SE}(Z\alpha)$ as $Z\alpha \to 0$. The higher-order terms in the potential expansion (see Fig. 3 below) and relativistic corrections to the wave function both generate terms of higher order in $Z\alpha$ which are manifest in Eq. (2.2) in the form of the nonvanishing function $G_{\rm SE}(Z\alpha)$, which summarizes the effects of the relativistic corrections to the bound electron wave function and of higher-order terms in the potential expansion. For very soft virtual photons, the potential expansion fails and generates an infrared divergence which is cut off by the atomic momentum scale $Z\alpha$. This cutoff for the *infrared* divergence is one of the mechanisms that leads to the logarithmic terms in Eq. (2.2). Some of the nonlogarithmic terms of relative order $(Z\alpha)^2$ in Eq. (2.2) are generated by the relativistic corrections to the wave function. The function $G_{\rm SE}$ does not vanish, but approaches a constant in the limit $Z\alpha \to 0$. This constant can be determined by analytic or semianalytic calculations; it is referred to as the A_{60} coefficient, i.e.,

$$A_{60}(nl_j) = G_{\rm SE}(nl_j, 0). \tag{2.14}$$

The evaluation of the coefficient $A_{60}(1S_{1/2})$ has been historically problematic [15,34–37]. For the $2S$ state, there is currently only one precise analytic result available (Ref. [15]),

$$A_{60}(2S_{1/2}) = -31.840\,47(1). \tag{2.15}$$

For the $2P_{1/2}$ state, the analytically obtained result is (Ref. [16])

$$A_{60}(2P_{1/2}) = -0.998\,91(1), \tag{2.16}$$

and for the $2P_{3/2}$ state, we have (Ref. [16])

$$A_{60}(2P_{3/2}) = -0.503\,37(1). \tag{2.17}$$

The analytic evaluations essentially rely on an expansion of the relativistic Dirac-Coulomb propagator in powers of the binding field, i.e., in powers of Coulomb interactions of the electron with the nucleus. In numerical evaluations, the binding field is treated nonperturbatively, and no expansion is performed.

B. Formulation of the numerical problem

Numerical cancellations are severe for small nuclear charges. In order to understand the origin of the numerical cancellations it is necessary to consider the renormalization of the self-energy. The renormalization procedure postulates that the self-energy is essentially the effect on the bound electron due to the self-interaction with its own radiation field, minus the same effect on a free electron which is absorbed in the mass of the electron and therefore not observable. The self-energy of the bound electron is the residual effect obtained after the subtraction of two large quantities. Terms associated with renormalization counterterms are of order 1 in the $Z\alpha$ expansion, whereas the residual effect is of order $(Z\alpha)^4$ [see Eq. (2.1)]. This corresponds to a loss of roughly nine significant digits at $Z=1$. Consequently, even the precise evaluation of the one-photon self-energy in a Coulomb field presented in [46] extends only down to $Z=5$. Among the self-energy corrections in one-loop and higher-loop order, numerical cancellations in absolute terms are most severe for the *one*-loop problem because of the large size of the effect of the one-loop self-energy correction on the spectrum.

For our high-precision numerical evaluation, we start from the regularized and renormalized expression for the one-loop self-energy of a bound electron,

$$\begin{aligned}\Delta E_{\rm SE} &= \lim_{\Lambda\to\infty}\left\{ i\,e^2\,{\rm Re}\int_{C_{\rm F}}\frac{d\omega}{2\pi}\int\frac{d\boldsymbol{k}}{(2\pi)^3}D_{\mu\nu}(k^2,\Lambda)\right.\\ &\left.\times\left\langle\overline{\psi}\right|\gamma^\mu\frac{1}{\not p-\not k-1-\gamma^0 V}\gamma^\nu\left|\psi\right\rangle-\Delta m\right\}\\ &= \lim_{\Lambda\to\infty}\left\{ -i\,e^2\,{\rm Re}\int_{\mathcal C}\frac{d\omega}{2\pi}\int\frac{d\boldsymbol{k}}{(2\pi)^3}D_{\mu\nu}(k^2,\Lambda)\right.\\ &\left.\times\langle\psi|\,\alpha^\mu\,e^{i\boldsymbol{k}\cdot\boldsymbol{x}}\,G(E_n-\omega)\,\alpha^\nu\,e^{-i\boldsymbol{k}\cdot\boldsymbol{x}}\,|\psi\rangle-\Delta m\right\},\end{aligned} \tag{2.18}$$

where G denotes the Dirac-Coulomb propagator,

$$G(z) = \frac{1}{\boldsymbol{\alpha}\cdot\boldsymbol{p}+\beta+V-z}, \tag{2.19}$$

and Δm is the Λ-dependent (cutoff-dependent) one-loop mass counter term,

$$\Delta m = \frac{\alpha}{\pi}\left(\tfrac{3}{4}\ln\Lambda^2+\tfrac{3}{8}\right)\langle\beta\rangle. \tag{2.20}$$

The photon propagator $D_{\mu\nu}(k^2,\Lambda)$ in Eq. (2.18) in Feynman gauge reads

$$D_{\mu\nu}(k^2,\Lambda) = -\left(\frac{g_{\mu\nu}}{k^2+i\,\epsilon}-\frac{g_{\mu\nu}}{k^2-\Lambda^2+i\,\epsilon}\right). \tag{2.21}$$

The contour $C_{\rm F}$ in Eq. (2.18) is the Feynman contour, whereas the contour $\mathcal{C}$ is depicted in Fig. 1. The contour $\mathcal{C}$ is employed for the ω integration in the current evaluation [see the last line of Eq. (2.18)]. The energy variable z in Eq. (2.19) therefore assumes the value

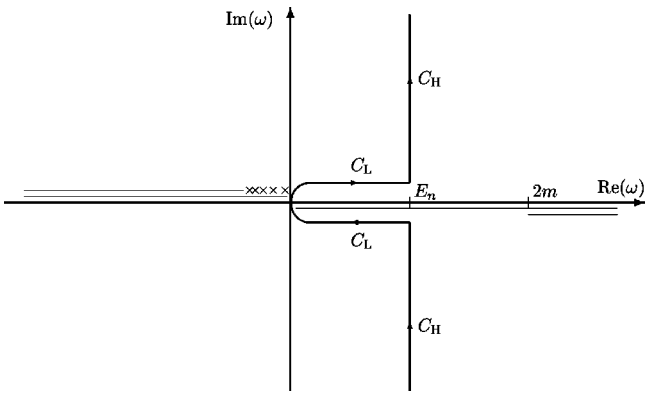

FIG. 1. Integration contour $\mathcal{C}$ for the integration over the energy $\omega=E_n-z$ of the virtual photon. The contour $\mathcal{C}$ consists of the low-energy contour C_L and the high-energy contour C_H. Lines shown displaced directly below and above the real axis denote branch cuts from the photon and electron propagator. Crosses denote poles originating from the discrete spectrum of the electron propagator. The contour used in this work corresponds to the one used in [47].

$$z=E_n-\omega, \tag{2.22}$$

where E_n is the Dirac energy of the atomic state, and ω denotes the complex-valued energy of the virtual photon. It is understood that the limit $\Lambda\to\infty$ is taken *after* all integrals in Eq. (2.18) are evaluated.

The integration contour for the complex-valued energy of the virtual photon ω in this calculation is the contour $\mathcal{C}$ employed in [46–49] and depicted in Fig. 1. The integrations along the low-energy contour C_L and the high-energy contour C_H in Fig. 1 give rise to the low- and the high-energy contributions ΔE_L and ΔE_H to the self-energy, respectively. Here, we employ a further separation of the low-energy integration contour C_L into an infrared contour C_{IR} and a middle-energy contour C_M shown in Fig. 2. This separation gives rise to a separation of the low-energy part ΔE_L into the infrared part ΔE_{IR} and the middle-energy part ΔE_M,

$$\Delta E_L=\Delta E_{IR}+\Delta E_M. \tag{2.23}$$

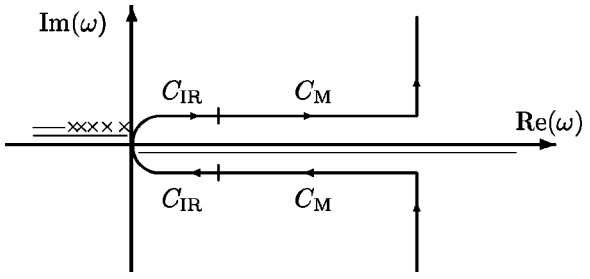

FIG. 2. Separation of the low-energy contour C_L into the infrared part C_{IR} and the middle-energy part C_M. As in Fig. 1, the lines directly above and below the real axis denote branch cuts from the photon and electron propagator. Strictly speaking, the figure is valid only for the ground state. For excited states, some of the crosses, which denote poles originating from the discrete spectrum of the electron propagator, are positioned to the right of the line $\mathrm{Re}\,\omega=0$. These poles are subtracted in the numerical evaluation.

For the low-Z systems discussed here, all complications that arise for excited states due to the decay into the ground state are relevant only for the infrared part. Except for the further separation into the infrared and the middle-energy part, the same basic formulation of the self-energy problem as in [47] is used. This leads to the following separation: for the infrared part ΔE_{IR},

$$\omega\in(0,\tfrac{1}{10}E_n)\pm i\,\delta,$$

for the middle-energy part ΔE_M,

$$\omega\in(\tfrac{1}{10}E_n,E_n)\pm i\,\delta,$$

and for the high-energy part ΔE_H,

$$\omega\in E_n+i\,(-\infty,+\infty).$$

Integration along these contours gives rise to the infrared, the middle-energy, and the high-energy contributions to the energy shift. For all of these contributions, lower-order terms are subtracted in order to obtain the contribution to the self-energy of order $(Z\alpha)^4$. We obtain for the infrared part,

$$\Delta E_{IR}=\frac{\alpha}{\pi}\left[\frac{21}{200}\langle\beta\rangle+\frac{43}{600}\langle V\rangle+\frac{(Z\alpha)^4}{n^3}F_{IR}(nl_j,Z\alpha)\right], \tag{2.24}$$

where $F_{IR}(nl_j,Z\alpha)$ is a dimensionless function of order one. The middle-energy part is recovered as

$$\Delta E_M=\frac{\alpha}{\pi}\left[\frac{279}{200}\langle\beta\rangle+\frac{219}{200}\langle V\rangle+\frac{(Z\alpha)^4}{n^3}F_M(nl_j,Z\alpha)\right], \tag{2.25}$$

and the high-energy part reads [47,48]

$$\Delta E_H=\Delta m+\frac{\alpha}{\pi}\left[-\frac{3}{2}\langle\beta\rangle-\frac{7}{6}\langle V\rangle+\frac{(Z\alpha)^4}{n^3}F_H(nl_j,Z\alpha)\right]. \tag{2.26}$$

The infrared part is discussed in Sec. III A. The middle-energy part is divided into a middle-energy subtraction term F_{MA} and a middle-energy remainder F_{MB}. The subtraction term F_{MA} is discussed in Sec. III B, the remainder term F_{MB} is treated in Sec. III C. We recover the middle-energy term as the sum

$$F_M(nl_j,Z\alpha)=F_{MA}(nl_j,Z\alpha)+F_{MB}(nl_j,Z\alpha). \tag{2.27}$$

A similar separation is employed for the high-energy part. The high-energy part is divided into a subtraction term F_{HA}, which is evaluated in Sec. IV A, and the high-energy remainder F_{HB}, which is discussed in Sec. IV B. The sum of the subtraction term and the remainder is

$$F_H(nl_j,Z\alpha)=F_{HA}(nl_j,Z\alpha)+F_{HB}(nl_j,Z\alpha). \tag{2.28}$$

The total energy shift is given as

$$\Delta E_{\rm SE}=\Delta E_{\rm IR}+\Delta E_{\rm M}+E_{\rm H}-\Delta m$$
$$=\frac{\alpha}{\pi}\frac{(Z\alpha)^4}{n^3}[F_{\rm IR}(nl_j,Z\alpha)$$
$$+F_{\rm M}(nl_j,Z\alpha)+F_{\rm H}(nl_j,Z\alpha)]. \qquad (2.29)$$

The scaled self-energy function F defined in Eq. (2.1) is therefore obtained as

$$F(nl_j,Z\alpha)=F_{\rm IR}(nl_j,Z\alpha)+F_{\rm M}(nl_j,Z\alpha)+F_{\rm H}(nl_j,Z\alpha). \qquad (2.30)$$

In analogy to the approach described in [46,47,49], we define the low-energy part as the sum of the infrared part and the middle-energy part,

$$\Delta E_{\rm L}=\Delta E_{\rm IR}+\Delta E_{\rm M}$$
$$=\frac{\alpha}{\pi}\left[\frac{3}{2}\langle\beta\rangle+\frac{7}{6}\langle V\rangle+\frac{(Z\alpha)^4}{n^3}F_{\rm L}(nl_j,Z\alpha)\right], \qquad (2.31)$$

where

$$F_{\rm L}(nl_j,Z\alpha)=F_{\rm IR}(nl_j,Z\alpha)+F_{\rm M}(nl_j,Z\alpha). \qquad (2.32)$$

The limits for the functions $F_{\rm L}(nl_j,Z\alpha)$ and $F_{\rm H}(nl_j,Z\alpha)$ as $Z\alpha\to 0$ were obtained in [5,48–50].

C. Treatment of the divergent terms

The free-electron propagator

$$F=\frac{1}{\boldsymbol{\alpha}\cdot\boldsymbol{p}+\beta-z} \qquad (2.33)$$

and the full electron propagator G defined in Eq. (2.19) fulfill the following identity, which is of particular importance for the validity of the method used in the numerical evaluation of the all-order binding correction to the Lamb shift,

$$G=F-F\,V\,F+F\,V\,G\,V\,F. \qquad (2.34)$$

This identity leads naturally to a separation of the one-photon self-energy into a zero-vertex, a single-vertex, and a many-vertex term. This is represented diagrammatically in Fig. 3.

All ultraviolet divergences which occur in the one-photon problem (mass counter term and vertex divergence) are generated by the zero-vertex and the single-vertex terms. The many-vertex term is ultraviolet safe. Of crucial importance is the observation that one may additionally simplify the problem by replacing the one-potential term with an approximate expression in which the potential is ''commuted to the outside.'' The approximate expression generates all divergences and all terms of lower order than $\alpha(Z\alpha)^4$ present in the one-vertex term. Unlike the raw one-potential term, it is amenable to significant further simplification and can be reduced to *one*-dimensional numerical integrals that can be evaluated easily (a straightforward formulation of the self-energy problem requires a *three*-dimensional numerical integration). Without this significant improvement, an all-order calculation would be much more difficult at low nuclear charge, because the lower-order terms would introduce significant further numerical cancellations.

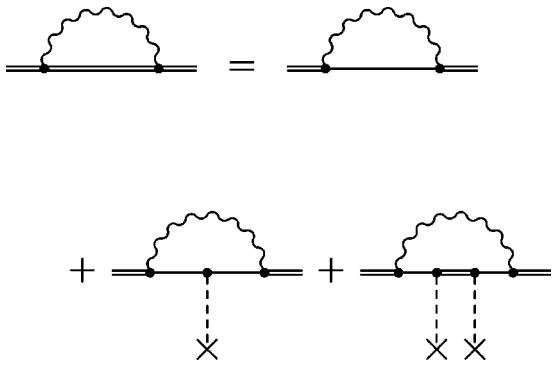

FIG. 3. The exact expansion of the bound electron propagator in powers of the binding field leads to a zero-potential, a one-potential, and a many-potential term. The dashed lines denote Coulomb photons; the crosses denote the interaction with the (external) binding field.

In addition, the special approximate resolvent can be used effectively for an efficient subtraction scheme in the middle-energy part of the calculation. In the infrared part, such a subtraction is not used because it would introduce infrared divergences.

We now turn to the construction of the special approximate resolvent, which will be referred to as $G_{\rm A}$ and will be used in this calculation to isolate the ultraviolet divergences in the high-energy part (and to provide subtraction terms in the middle-energy part). It is based on an approximation to the first two terms on the right-hand side of Eq. (2.34). The so-called one-potential term FVF in Eq. (2.34) is approximated by an expression in which the potential terms V are commuted to the outside:

$$-FVF\approx-\tfrac{1}{2}\{V,F^2\}. \qquad (2.35)$$

Furthermore, the following identity is used:

$$F^2=\left(\frac{1}{\boldsymbol{\alpha}\cdot\boldsymbol{p}+\beta-z}\right)^2$$
$$=\frac{1}{\boldsymbol{p}^2+1-z^2}+\frac{2\,z\,(\beta+z)}{(\boldsymbol{p}^2+1-z^2)^2}+\frac{2\,z\,(\boldsymbol{\alpha}\cdot\boldsymbol{p})}{(\boldsymbol{p}^2+1-z^2)^2}. \qquad (2.36)$$

In 2×2 spinor space, this expression may be divided into a diagonal and a nondiagonal part. The diagonal part is

$$\mathrm{diag}(F^2)=\frac{1}{\boldsymbol{p}^2+1-z^2}+\frac{2\,z\,(\beta+z)}{(\boldsymbol{p}^2+1-z^2)^2}. \qquad (2.37)$$

The off-diagonal part is given by

$$F^2 - \mathrm{diag}(F^2) = \frac{2\,z\,(\boldsymbol{\alpha}\cdot\boldsymbol{p})}{(\boldsymbol{p}^2+1-z^2)^2}.$$

We define the resolvent G_{A} as

$$G_{\mathrm{A}} = F - \tfrac{1}{2}\,\{V, \mathrm{diag}(F^2)\}. \tag{2.38}$$

All divergences that occur in the self-energy are generated by the simplified propagator G_{A}. We define the propagator G_{B} as the difference of G and G_{A},

$$G_{\mathrm{B}} = G - G_{\mathrm{A}} = \tfrac{1}{2}\,\{V, \mathrm{diag}(F^2)\} - F\,V\,F + F\,V\,G\;V\,F. \tag{2.39}$$

G_{B} does not generate any divergences and leads to the middle-energy remainder discussed in Sec. III C and the high-energy remainder (Sec. IV B).

III. THE LOW-ENERGY PART

A. The infrared part

The infrared part is given by

$$\Delta E_{\mathrm{IR}} = -i\,e^2\,\mathrm{Re}\int_{C_{\mathrm{IR}}}\frac{d\omega}{2\pi}\int\frac{d\boldsymbol{k}}{(2\pi)^3}D_{\mu\nu}(k^2) \times\langle\psi|\,\alpha^\mu\,e^{i\,\boldsymbol{k}\cdot\boldsymbol{x}}\,G(E_n-\omega)\,\alpha^\nu\,e^{-i\,\boldsymbol{k}\cdot\boldsymbol{x}}\,|\psi\rangle, \tag{3.1}$$

where relevant definitions of the symbols can be found in Eqs. (2.18)–(2.21), the contour C_{IR} is as shown in Fig. 2, and the unregularized version of the photon propagator

$$D_{\mu\nu}(k^2) = -\frac{g_{\mu\nu}}{k^2 + i\,\epsilon} \tag{3.2}$$

may be used. The infrared part consists of the following integration region for the virtual photon:

$$\omega \in (0, \tfrac{1}{10}\,E_n) \pm i\,\delta$$
$$z \in (\tfrac{9}{10}\,E_n, E_n) \pm i\,\delta. \tag{3.3}$$

Following Secs. 2 and 3 of [47], we write ΔE_{IR} as a three-dimensional integral [see, e.g., Eqs. (3.4), (3.11), and (3.14) of [47]]

$$\Delta E_{\mathrm{IR}} = \frac{\alpha}{\pi}\,\frac{E_n}{10} - \frac{\alpha}{\pi}\mathrm{P}\int_{(9/10)\,E_n}^{E_n} dz \int_0^\infty dx_1\,x_1^2 \times\int_0^\infty dx_2\,x_2^2\,\mathcal{M}_{\mathrm{IR}}(x_2,x_1,z), \tag{3.4}$$

where P is the principal value and where

$$\mathcal{M}_{\mathrm{IR}}(x_2,x_1,z) = \sum_\kappa \sum_{i,j=1}^{2} f_{\bar{\imath}}(x_2)\,G_\kappa^{ij}(x_2,x_1,z) \times f_{\bar{\jmath}}(x_1)\,A_\kappa^{ij}(x_2,x_1). \tag{3.5}$$

Here, the quantum number κ is the Dirac angular quantum number of the intermediate state,

$$\kappa = 2\,(l-j)\,(j+\tfrac{1}{2}), \tag{3.6}$$

where l is the orbital angular momentum quantum number and j is the total angular momentum of the bound electron. The functions $f_i(x_2)$ $(i=1,2)$ are the radial wave functions defined in Eq. (A.4) in [47] for an arbitrary bound state [and in Eq. (A.8) in [47] for the $1S$ state]. We define $\bar{\imath} = 3-i$. The functions $G_\kappa^{ij}(x_2,x_1,z)$ $(i,j=1,2)$ are the radial Green functions, which result from a decomposition of the electron Green function defined in Eq. (2.19) into partial waves. The explicit formulas are given in Eq. (A.16) in [47].

The photon angular functions A_κ^{ij} $(i,j=1,2)$ are defined in Eq. (3.15) of Ref. [47] for an arbitrary bound state. In Eq. (3.17) in [47], specific formulas are given for the $1S$ state. In Eqs. (2.2), (2.3), and (2.4) of [49], the special cases of $S_{1/2}$, $P_{1/2}$, and $P_{3/2}$ states are considered. Further relevant formulas for excited states can be found in [51]. The photon angular functions depend on the energy argument z, but this dependence is usually suppressed. The summation over κ in Eq. (3.5) extends over all negative and all positive integers, excluding zero. We observe that the integral is symmetric under the interchange of the radial coordinates x_2 and x_1, so that

$$\Delta E_{\mathrm{IR}} = \frac{\alpha}{\pi}\,\frac{E_n}{10} - \frac{2\,\alpha}{\pi}\mathrm{P}\int_{(9/10)\,E_n}^{E_n} dz \int_0^\infty dx_1\,x_1^2 \times\int_0^{x_1} dx_2\,x_2^2\,\mathcal{M}_{\mathrm{IR}}(x_2,x_1,z). \tag{3.7}$$

The following variable substitution:

$$r = x_2/x_1, \quad y = a\,x_1 \tag{3.8}$$

is made, so that $r \in (0,1)$ and $y \in (0,\infty)$. The scaling variable a is defined as

$$a = 2\,\sqrt{1-E_n^2}. \tag{3.9}$$

The Jacobian is

$$\left|\frac{\partial(x_2,x_1)}{\partial(r,y)}\right| = \begin{vmatrix} \dfrac{\partial x_2}{\partial r} & \dfrac{\partial x_1}{\partial r} \\ \dfrac{\partial x_2}{\partial y} & \dfrac{\partial x_1}{\partial y} \end{vmatrix} = \frac{y}{a^2}. \tag{3.10}$$

The function S_{IR} is given by

$$S_{\mathrm{IR}}(r,y,z) = -\frac{2\,r^2\,y^5}{a^6}\,\mathcal{M}_{\mathrm{IR}}\left(\frac{r\,y}{a},\frac{y}{a},z\right) = -\frac{2\,r^2\,y^5}{a^6}\sum_{|\kappa|=1}^{\infty}\sum_{\kappa=\pm|\kappa|}\sum_{i,j=1}^{2} f_{\bar{\imath}}\left(\frac{r\,y}{a}\right) \times G_\kappa^{ij}\left(\frac{r\,y}{a},\frac{y}{a},z\right) f_{\bar{\jmath}}\left(\frac{y}{a}\right) A_\kappa^{ij}\left(\frac{r\,y}{a},\frac{y}{a}\right)$$

$$= -\frac{2\,r^2\,y^5}{a^6}\sum_{|\kappa|=1}^{\infty} T_{\mathrm{IR},|\kappa|}(r,y,z), \tag{3.11}$$

where in the last line we define implicitly the terms $T_{\mathrm{IR},|\kappa|}$ for $|\kappa|=1,\ldots,\infty$ as

$$T_{\mathrm{IR},|\kappa|}(r,y,z)=\sum_{\kappa=\pm|\kappa|}\sum_{i,j=1}^{2} f_{\bar{\imath}}\left(\frac{r\,y}{a}\right) G_{\kappa}^{ij}\left(\frac{r\,y}{a},\frac{y}{a},z\right) \times f_{\bar{J}}\left(\frac{y}{a}\right) A_{\kappa}^{ij}\left(\frac{r\,y}{a},\frac{y}{a}\right). \tag{3.12}$$

Using the definition (3.11), we obtain for ΔE_{IR},

$$\Delta E_{\mathrm{IR}}=\frac{\alpha}{\pi}\frac{E_n}{10}+\frac{\alpha}{\pi}\mathrm{P}\int_{(9/10)\,E_n}^{E_n} dz\int_0^1 dr\int_0^{\infty} dy\, S_{\mathrm{IR}}(r,y,z). \tag{3.13}$$

The specification of the principal value (P) is necessary for the excited states of the L shell because of the poles along the integration contour which correspond to the spontaneous decay into the ground state. Here we are exclusively concerned with the real part of the energy shift, as specified in Eq. (3.1), which is equivalent to the specification of the principal value in Eq. (3.13). Evaluation of the integral over z is facilitated by the subtraction of those terms that generate the singularities along the integration contour (for higher excited states, there can be numerous bound-state poles, as pointed out in [51,52]). For the $2S$ and $2P_{1/2}$ states, only the pole contribution from the ground state must be subtracted. For the $2P_{3/2}$ state, pole contributions originating from the $1S$, the $2S$, and the $2P_{1/2}$ states must be taken into account. The numerical evaluation of the subtracted integrand proceeds along ideas outlined in [49,51] and is not discussed here in any further detail.

The scaling parameter a for the integration over y is chosen to simplify the exponential dependence of the function S defined in Eq. (3.11). The main exponential dependence is given by the relativistic radial wave functions (upper and lower components). Both components $[f_1(x)$ and $f_2(x)]$ vary approximately as (neglecting relatively slowly varying factors)

$$\exp(-a\,x/2) \quad \text{(for large } x\text{)}.$$

The scaling variable a, expanded in powers of $Z\alpha$, is

$$\begin{aligned} a &= 2\,\sqrt{1-E_n^2} \\ &= 2\,\sqrt{1-\left(1-\frac{(Z\alpha)^2}{2\,n^2}+O[(Z\alpha)^4]\right)^2} \\ &= 2\,\frac{Z\alpha}{n}+O[(Z\alpha)^3]. \end{aligned} \tag{3.14}$$

Therefore, a is just twice the *inverse* of the Bohr radius $n/(Z\alpha)$ in the nonrelativistic limit. The product

$$f_{\bar{\imath}}\left(\frac{ry}{a}\right)\times f_{\bar{J}}\left(\frac{y}{a}\right) \quad \text{for arbitrary } \overline{\imath,J}\in\{1,2\}$$

[which occurs in Eq. (3.11)] depends on the radial arguments approximately as

$$e^{-y}\times\exp[\tfrac{1}{2}\,(1-r)\,y] \quad \text{(for large } y\text{)}.$$

Note that the main dependence as given by the term $\exp(-y)$ is exactly the weight factor of the Gauss-Laguerre integration quadrature formula. The deviation from the exact $\exp(-y)$-type behavior becomes smaller as $r\to 1$. This is favorable because the region near $r=1$ gives a large contribution to the integral in Eq. (3.13).

The sum over $|\kappa|$ in Eq. (3.11) is carried out locally, i.e., for each set of arguments r,y,z. The sum over $|\kappa|$ is absolutely convergent. For $|\kappa|\to\infty$, the convergence of the sum is governed by the asymptotic behavior of the Bessel functions that occur in the photon functions A_{κ}^{ij} $(i,j=1,2)$ [see Eqs. (3.15) and (3.16) in [47]]. The photon functions contain products of two Bessel functions of the form $\mathcal{J}_l(\rho_{2/1})$, where $\mathcal{J}_l$ stands for either j_l or j_l', and the index l is in the range $l\in\{|\kappa|-1,|\kappa|,|\kappa|+1\}$. The argument is either $\rho_2=(E_n-z)\,x_2$ or $\rho_1=(E_n-z)\,x_1$. The asymptotic behavior of the two relevant Bessel functions for large l (and therefore large $|\kappa|$) is

$$j_l'(x)=\frac{l}{x}\,\frac{x^l}{(2l+1)!!}\left[1+O\left(\frac{1}{l}\right)\right] \tag{3.15}$$

and

$$j_l(x)=\frac{x^l}{(2l+1)!!}\left[1+O\left(\frac{1}{l}\right)\right]. \tag{3.16}$$

This implies that when $\min\{\rho_2,\rho_1\}=\rho_2<l$, the function $\mathcal{J}_l(\rho_2)$ vanishes with increasing l approximately as $(e\,\rho_2/2l)^l$. This rapidly converging asymptotic behavior sets in as soon as $l\approx|\kappa|>\rho_2=r\,\omega\,y/a$ [see Eqs. (2.22) and (3.12)]. Due to the rapid convergence for $|\kappa|>\rho_2$, the maximum angular-momentum quantum number $|\kappa|$ in the numerical calculation of the infrared part is less than 3000. Note that because $z\in(\frac{9}{10}\,E_n,E_n)$ in the infrared part, $\omega<\frac{1}{10}\,E_n$.

The integration scheme is based on a crude estimate of the dependence of the integrand $S_{\mathrm{IR}}(r,y,z)$ defined in Eq. (3.11) on the integration variables r, y, and z. The main contribution to the integral is given by the region where the arguments of the Whittaker functions as they occur in the Green function [see Eq. (A.16) in [47]] are much larger than the Dirac angular momentum,

$$2\,c\,\frac{y}{a}\gg|\kappa|$$

(see also p. 56 of [48]). We assume the asymptotic form of the Green function given in Eq. (A.3) in [48] applies, and we attribute a factor

TABLE I. Infrared part for the K- and L-shell states, $F_{\rm IR}(1S_{1/2},Z\alpha)$, $F_{\rm IR}(2S_{1/2},Z\alpha)$, $F_{\rm IR}(2P_{1/2},Z\alpha)$, and $F_{\rm IR}(2P_{3/2},Z\alpha)$, evaluated for low-$Z$ hydrogenlike ions. The calculations were performed with the numerical value of $\alpha^{-1}=137.036$ for the fine-structure constant.

Z	$F_{\rm IR}(1S_{1/2},Z\alpha)$	$F_{\rm IR}(2S_{1/2},Z\alpha)$	$F_{\rm IR}(2P_{1/2},Z\alpha)$	$F_{\rm IR}(2P_{3/2},Z\alpha)$
1	7.236 623 736 8(1)	7.479 764 180(1)	0.085 327 852(1)	0.082 736 497(1)
2.	5.539 002 119 1(1)	5.782 025 637(1)	0.086 073 669(1)	0.083 279 461(1)
3	4.598 155 821 8(1)	4.840 923 962(1)	0.087 162 510(1)	0.084 091 830(1)
4	3.963 124 140 6(1)	4.205 501 798(1)	0.088 543 188(1)	0.085 140 788(1)
5	3.493 253 319 4(1)	3.735 114 958(1)	0.090 180 835(1)	0.086 403 178(1)

$$\exp[-(1-r)\,c\,y/a]$$

to the radial Green functions G_κ^{ij} as they occur in Eq. (3.11). Note that relatively slowly varying factors are replaced by unity. The products of the radial wave functions f_i^- and f_j^-, according to the discussion following Eq. (3.14), behave as

$$e^{-y}\exp[\tfrac{1}{2}\,(1-r)\,y]$$

for large y. The photon functions A_κ^{ij} in Eq. (3.11) give rise to an approximate factor

$$\frac{\sin[(1-r)\,(E_n-z)\,y/a]}{(1-r)}. \tag{3.17}$$

Therefore [see also Eq. (2.12) in [48]], we base our choice of the integration routine on the approximation

$$e^{-y}\exp\left[-\left(\frac{c}{a}-\frac{1}{2}\right)(1-r)\,y\right]\times\frac{\sin[(1-r)\,(E_n-z)\,y/a]}{(1-r)} \tag{3.18}$$

for $S_{\rm IR}$. The three-dimensional integral in Eq. (3.13) is evaluated by successive Gaussian quadrature. Details of the integration procedure can be found in [5].

In order to check the numerical stability of the results, the calculations are repeated with three different values of the fine-structure constant α,

$$\alpha_< = 1/137.036\,000\,5,$$
$$\alpha_0 = 1/137.036\,000\,0, \tag{3.19}$$

and

$$\alpha_> = 1/137.035\,999\,5.$$

These values are close to the 1998 CODATA recommended value of $\alpha^{-1}=137.035\,999\,76(50)$ [53]. The calculation was parallelized using the message passing interface (MPI) and carried out on a cluster of Silicon Graphics workstations and on an IBM 9276 SP/2 multiprocessor system [54]. The results for the infrared part $F_{\rm IR}$, defined in Eq. (2.24), are given in Table I for a value of $\alpha^{-1}=\alpha_0^{-1}=137.036$. This value of α will be used exclusively in the numerical evaluations presented here. For numerical results obtained by employing the values of $\alpha_<$ and $\alpha_>$ [see Eq. (3.19)] we refer to [5].

B. The middle-energy subtraction term

The middle-energy part is given by

$$\Delta E_{\rm M} = -i\,e^2\int_{C_{\rm M}}\frac{d\omega}{2\pi}\int\frac{d^3\boldsymbol{k}}{(2\pi)^3}D_{\mu\nu}(k^2) \times\langle\psi|\,\alpha^\mu\,e^{i\,\boldsymbol{k}\cdot\boldsymbol{x}}G(E_n-\omega)\,\alpha^\nu\,e^{-i\,\boldsymbol{k}\cdot\boldsymbol{x}}|\psi\rangle, \tag{3.20}$$

where relevant definitions of the symbols can be found in Eqs. (2.18)–(2.21) and Eq. (3.2), and the contour $C_{\rm M}$ is as shown in Fig. 2. The middle-energy part consists of the following integration region for the virtual photon:

$$\omega\in(\tfrac{1}{10}\,E_n,E_n)\pm i\,\delta$$
$$z\in(0,\tfrac{9}{10}\,E_n)\pm i\,\delta. \tag{3.21}$$

The numerical evaluation of the middle-energy part is simplified considerably by the decomposition of the relativistic Dirac-Coulomb Green function G as

$$G=G_{\rm A}+G_{\rm B}, \tag{3.22}$$

where $G_{\rm A}$ is defined in Eq. (2.38) and represents the sum of an approximation to the so-called zero- and one-potential terms generated by the expansion of the Dirac-Coulomb Green function G in powers of the binding field V. We define the middle-energy subtraction term $F_{\rm MA}$ as the expression obtained upon substitution of the propagator $G_{\rm A}$ for G in Eq. (3.20). The propagator $G_{\rm B}$ is simply calculated as the difference of G and $G_{\rm A}$ [see Eq. (2.39)]. A substitution of the propagator $G_{\rm B}$ for G in Eq. (3.20) leads to the middle-energy remainder $F_{\rm MB}$ which is discussed in Sec. III C. We provide here the explicit expressions

$$\Delta E_{\rm MA} = -i\,e^2\int_{C_{\rm M}}\frac{d\omega}{2\pi}\int\frac{d\boldsymbol{k}}{(2\pi)^3}D_{\mu\nu}(k^2) \times\langle\psi|\,\alpha^\mu\,e^{i\,\boldsymbol{k}\cdot\boldsymbol{x}}\,G_{\rm A}(E_n-\omega)\,\alpha^\nu\,e^{-i\,\boldsymbol{k}\cdot\boldsymbol{x}}|\psi\rangle \tag{3.23}$$

and

$$\Delta E_{\rm MB} = -i\,e^2 \int_{C_{\rm M}} \frac{d\omega}{2\pi} \int \frac{d^3\boldsymbol{k}}{(2\pi)^3} D_{\mu\nu}(k^2) \times \langle\psi|\,\alpha^\mu\, e^{i\,\boldsymbol{k}\cdot\boldsymbol{x}}\, G_{\rm B}(E_n-\omega)\,\alpha^\nu\, e^{-i\,\boldsymbol{k}\cdot\boldsymbol{x}}\,|\psi\rangle. \tag{3.24}$$

Note that the decomposition of the Dirac-Coulomb Green function as in Eq. (3.22) is not applicable in the infrared part because of numerical problems for ultrasoft photons (infrared divergences). Rewriting Eq. (3.23) appropriately into a three-dimensional integral [5,47,48], we have

$$\Delta E_{\rm MA} = \frac{\alpha}{\pi}\frac{9}{10}E_n - \frac{2\,\alpha}{\pi}\int_0^{(9/10)\,E_n} dz \int_0^\infty dx_1\, x_1^2 \times \int_0^{x_1} dx_2\, x_2^2\, \mathcal{M}_{\rm MA}(x_2,x_1,z). \tag{3.25}$$

The function $\mathcal{M}_{\rm MA}(x_2,x_1,z)$ is defined in analogy to the function $\mathcal{M}_{\rm IR}(x_2,x_1,z)$ defined in Eq. (3.5) for the infrared part. Also, we define a function $\mathcal{S}_{\rm MA}(x_2,x_1,z)$ in analogy to the function $\mathcal{S}_{\rm IR}(x_2,x_1,z)$ given in Eq. (3.11) for the infrared part, which will be used in Eq. (3.28) below. We have

$$\begin{aligned} S_{\rm MA}(r,y,z) &= -\frac{2\,r^2\,y^5}{a^6}\,\mathcal{M}_{\rm MA}\left(\frac{r\,y}{a},\frac{y}{a},z\right) \\ &= -\frac{2\,r^2\,y^5}{a^6}\sum_{|\kappa|=1}^{\infty}\sum_{\kappa=\pm|\kappa|}\sum_{i,j=1}^{2} f_i\left(\frac{r\,y}{a}\right) \times G^{ij}_{{\rm A},\kappa}\left(\frac{r\,y}{a},\frac{y}{a},z\right) f_J\left(\frac{y}{a}\right) A^{ij}_{\kappa}\left(\frac{r\,y}{a},\frac{y}{a}\right) \\ &= -\frac{2\,r^2\,y^5}{a^6}\sum_{|\kappa|=1}^{\infty} T_{{\rm MA},|\kappa|}(r,y,z). \end{aligned} \tag{3.26}$$

The expansion of the propagator $G_{\rm A}$ into partial waves is given in Eqs. (5.4) and (A.20) in [47] and in Eqs. (D.37) and (D.42) in [5]. This expansion leads to the component functions $G^{ij}_{{\rm A},\kappa}$. The terms $T_{{\rm MA},|\kappa|}$ in the last line of Eq. (3.26) read

$$T_{{\rm MA},|\kappa|}(r,y,z) = \sum_{\kappa=\pm|\kappa|}\sum_{i,j=1}^{2} f_i\left(\frac{r\,y}{a}\right) G^{ij}_{{\rm A},\kappa}\left(\frac{r\,y}{a},\frac{y}{a},z\right) \times f_J\left(\frac{y}{a}\right) A^{ij}_{\kappa}\left(\frac{r\,y}{a},\frac{y}{a}\right). \tag{3.27}$$

With these definitions, the middle-energy subtraction term $\Delta E_{\rm MA}$ can be written as

$$\Delta E_{\rm MA} = \frac{\alpha}{\pi}\frac{9}{10}E_n + \frac{\alpha}{\pi}\int_0^{(9/10)\,E_n} dz \int_0^\infty dy \int_0^1 dr\, S_{\rm MA}(r,y,z). \tag{3.28}$$

The subtracted lower-order terms yield

$$\Delta E_{\rm MA} = \frac{\alpha}{\pi}\left[\frac{279}{200}\langle\beta\rangle + \frac{219}{200}\langle V\rangle + \frac{(Z\alpha)^4}{n^3}F_{\rm MA}(nl_j,Z\alpha)\right]. \tag{3.29}$$

The three-dimensional integral in Eq. (3.28) is evaluated by successive Gaussian quadrature. Details of the integration procedure can be found in [5]. The numerical results are summarized in Table II.

C. The middle-energy remainder

The remainder term in the middle-energy part involves the propagator $G_{\rm B}$ defined in Eq. (2.39), $G_{\rm B}=G-G_{\rm A}$, where G is defined in Eq. (2.19) and $G_{\rm A}$ is given in Eq. (2.38). In analogy to the middle-energy subtraction term, the middle-energy remainder can be rewritten as a three-dimensional integral,

$$\Delta E_{\rm MB} = \frac{\alpha}{\pi}\int_0^{(9/10)\,E_n} dz \int_0^1 dr \int_0^\infty dy\, S_{\rm MB}(r,y,z), \tag{3.30}$$

where

$$S_{\rm MB}(r,y,z) = -\frac{2\,r^2\,y^5}{a^6}\sum_{|\kappa|=1}^{\infty}\sum_{\kappa=\pm|\kappa|}\sum_{i,j=1}^{2} f_i\left(\frac{r\,y}{a}\right) \times G^{ij}_{{\rm B},\kappa}\left(\frac{r\,y}{a},\frac{y}{a},z\right) f_J\left(\frac{y}{a}\right) A^{ij}_{\kappa}\left(\frac{r\,y}{a},\frac{y}{a}\right). \tag{3.31}$$

The functions $G^{ij}_{{\rm B},\kappa}$ are obtained as the difference of the expansion of the full propagator G and the simplified propagator $G_{\rm A}$ into angular momenta,

$$G^{ij}_{{\rm B},\kappa} = G^{ij}_{\kappa} - G^{ij}_{{\rm A},\kappa}, \tag{3.32}$$

where the G^{ij}_{κ} are listed in Eq. (A.16) in [47] and in Eq. (D.43) in [5], and the $G^{ij}_{{\rm A},\kappa}$ have already been defined in Eqs. (5.4) and (A.20) in [47] and in Eqs. (D.37) and (D.42) in [5]. There are no lower-order terms to subtract, and therefore

$$\Delta E_{\rm MB} = \frac{\alpha\,(Z\alpha)^4}{\pi\quad n^3}F_{\rm MB}(nl_j,Z\alpha). \tag{3.33}$$

The three-dimensional integral (3.30) is evaluated by successive Gaussian quadrature. Details of the integration procedure are provided in [5]. Numerical results for the middle-energy remainder $F_{\rm MB}$ are summarized in Table II for the K- and L-shell states.

For the middle-energy part, the separation into a subtraction and a remainder term has considerable computational advantages that become obvious upon inspection of Eqs. (3.29) and (3.33). The subtraction involves a propagator whose angular components can be evaluated by recursion [5,48], which is not computationally time consuming. Because the subtraction term involves lower-order components [see Eq. (2.25)], it has to be evaluated to high precision

TABLE II. Numerical results for the middle-energy subtraction term $F_{\rm MA}$, the middle-energy remainder term $F_{\rm MB}$, and the middle-energy term $F_{\rm M}$. The middle-energy term $F_{\rm M}$ is given as the sum $F_{\rm M}(nl_j,Z\alpha)=F_{\rm MA}(nl_j,Z\alpha)+F_{\rm MB}(nl_j,Z\alpha)$ [see also Eqs. (2.25), (3.29), and (3.33)].

Z	$F_{\rm MA}(1S_{1/2},Z\alpha)$	$F_{\rm MA}(2S_{1/2},Z\alpha)$	$F_{\rm MA}(2P_{1/2},Z\alpha)$	$F_{\rm MA}(2P_{3/2},Z\alpha)$
1	2.699 379 904 5(1)	2.720 878 318(1)	0.083 207 314(1)	0.701 705 240(1)
2	2.659 561 381 1(1)	2.681 820 660(1)	0.084 208 832(1)	0.701 850 024(1)
3	2.623 779 453 0(1)	2.647 262 568(1)	0.085 831 658(1)	0.702 091 147(1)
4	2.591 151 010 1(1)	2.616 290 432(1)	0.088 040 763(1)	0.702 426 850(1)
5	2.561 096 522 1(1)	2.588 297 638(1)	0.090 803 408(1)	0.702 854 461(1)
Z	$F_{\rm MB}(1S_{1/2},Z\alpha)$	$F_{\rm MB}(2S_{1/2},Z\alpha)$	$F_{\rm MB}(2P_{1/2},Z\alpha)$	$F_{\rm MB}(2P_{3/2},Z\alpha)$
1	1.685 993 923 2(1)	1.784 756 705(2)	0.771 787 771(2)	−0.094 272 681(2)
2	1.626 842 294 5(1)	1.725 583 798(2)	0.770 778 394(2)	−0.094 612 071(2)
3	1.571 406 090 7(1)	1.670 086 996(2)	0.769 153 314(2)	−0.095 165 248(2)
4	1.519 082 768 6(1)	1.617 650 004(2)	0.766 954 435(2)	−0.095 922 506(2)
5	1.469 482 409 0(1)	1.567 873 140(2)	0.764 220 149(2)	−0.096 874 556(2)
Z	$F_{\rm M}(1S_{1/2},Z\alpha)$	$F_{\rm M}(2S_{1/2},Z\alpha)$	$F_{\rm M}(2P_{1/2},Z\alpha)$	$F_{\rm M}(2P_{3/2},Z\alpha)$
1	4.385 373 827 7(1)	4.505 635 023(2)	0.854 995 085(2)	0.607 432 559(2)
2	4.286 403 675 7(1)	4.407 404 458(2)	0.854 987 226(2)	0.607 237 953(2)
3	4.195 185 543 6(1)	4.317 349 564(2)	0.854 984 972(2)	0.606 925 899(2)
4	4.110 233 778 8(1)	4.233 940 436(2)	0.854 995 198(2)	0.606 504 344(2)
5	4.030 578 931 1(1)	4.156 170 778(2)	0.855 023 557(2)	0.605 979 905(2)

numerically (in a typical case, a relative uncertainty of 10^{-19} is required). This high precision requires in turn a large number of integration points for the Gaussian quadratures, which is possible only if the numerical evaluation of the integrand is not computationally time consuming. For the remainder term, no lower-order terms have to be subtracted, and the relative precision required of the integrals is in the range of $10^{-11}\cdots10^{-9}$. A numerical evaluation to this lower level of precision is feasible, although the calculation of the Green function $G_{\rm B}$ is computationally more time consuming than that of $G_{\rm A}$ [5,47,48]. The separation of the high-energy part into a subtraction term and a remainder term, which is discussed in Sec. IV, is motivated by analogous considerations as for the middle-energy part. In the high-energy part, this separation is even more important than in the middle-energy part because of the occurrence of infinite terms that need to be subtracted analytically before a numerical evaluation can proceed [see Eq. (4.8) below].

We now summarize the results for the middle-energy part. The middle-energy part is the sum of the middle-energy subtraction term $F_{\rm MA}$ and the middle-energy remainder $F_{\rm MB}$ [see also Eq. (2.27)]. Numerical results are summarized in Table II for the K- and L-shell states. The low-energy part $F_{\rm L}$ is defined as the sum of the infrared contribution $F_{\rm IR}$ and the middle-energy contribution $F_{\rm M}$ [see Eq. (2.32)]. The results for $F_{\rm L}$ are provided in Table III for the K- and L-shell states. The limits for the low-energy part as a function of the bound-state quantum numbers can be found in Eq. (7.80) of [5]:

$$F_{\rm L}(nl_j,Z\alpha)=\frac{4}{3}\,\delta_{l,0}\ln(Z\alpha)^{-2}-\frac{4}{3}\ln k_0(n,l)+\left(\ln 2-\frac{11}{10}\right)\frac{1}{n}+\left(2\ln 2-\frac{16}{15}\right)\frac{1}{2\,l+1}+\left(\frac{3}{2}\ln 2-\frac{7}{4}\right)\times\frac{1}{\kappa\,(2\,l+1)}+\left(-\frac{3}{2}\ln 2+\frac{9}{4}\right)\frac{1}{|\kappa|}+\left(\frac{4}{3}\ln 2-\frac{1}{3}\right)\delta_{l,0}+\left(\ln 2-\frac{5}{6}\right)\frac{n-2\,l-1}{n\,(2\,l+1)}$$

TABLE III. Low-energy part $F_{\rm L}$ for the K- and L-shell states $F_{\rm L}(1S_{1/2},Z\alpha)$, $F_{\rm L}(2S_{1/2},Z\alpha)$, $F_{\rm L}(2P_{1/2},Z\alpha)$, and $F_{\rm L}(2P_{3/2},Z\alpha)$, evaluated for low-$Z$ hydrogenlike ions.

Z	$F_{\rm L}(1S_{1/2},Z\alpha)$	$F_{\rm L}(2S_{1/2},Z\alpha)$	$F_{\rm L}(2P_{1/2},Z\alpha)$	$F_{\rm L}(2P_{3/2},Z\alpha)$
1	11.621 997 564 5(1)	11.985 399 203(2)	0.940 322 937(2)	0.690 169 056(2)
2	9.825 405 794 7(1)	10.189 430 095(2)	0.941 060 895(2)	0.690 517 414(2)
3	8.793 341 365 4(1)	9.158 273 526(2)	0.942 147 482(2)	0.691 017 729(2)
4	8.073 357 919 4(1)	8.439 442 234(2)	0.943 538 386(2)	0.691 645 132(2)
5	7.523 832 250 6(1)	7.891 285 736(2)	0.945 204 392(2)	0.692 383 083(2)

$$+O(Z\alpha). \tag{3.34}$$

The limits for the states under investigation in this paper are

$$F_{\rm L}(1S_{1/2},Z\alpha)=(4/3)\ln(Z\alpha)^{-2}-1.554\,642+O(Z\alpha),$$

$$F_{\rm L}(2S_{1/2},Z\alpha)=(4/3)\ln(Z\alpha)^{-2}-1.191\,497+O(Z\alpha),$$

$$F_{\rm L}(2P_{1/2},Z\alpha)=0.940\,022+O(Z\alpha),$$

$$F_{\rm L}(2P_{3/2},Z\alpha)=0.690\,022+O(Z\alpha). \tag{3.35}$$

These limits are consistent with the numerical data in Table III. For S states, the low-energy contribution $F_{\rm L}$ diverges logarithmically as $Z\alpha\to 0$, whereas for P states, $F_{\rm L}$ approaches a constant as $Z\alpha\to 0$. The leading logarithm is a consequence of an infrared divergence cut off by the atomic momentum scale. It is a nonrelativistic effect which is generated by the nonvanishing probability density of S waves at the origin in the nonrelativistic limit. The presence of the logarithmic behavior for S states [nonvanishing A_{41} coefficient, see Eqs. (2.2) and (2.3)] and its absence for P states is reproduced consistently by the data in Table III.

IV. THE HIGH-ENERGY PART

A. The high-energy subtraction term

The high-energy part is given by

$$\Delta E_{\rm H}=-\lim_{\Lambda\to\infty} i\,e^2\int_{C_{\rm H}}\frac{d\omega}{2\pi}\int\frac{d\boldsymbol{k}}{(2\pi)^3}D_{\mu\nu}(k^2,\Lambda)\times\langle\psi|\,\alpha^\mu\,e^{i\,\boldsymbol{k}\cdot\boldsymbol{x}}\,G(E_n-\omega)\,\alpha^\nu\,e^{-i\,\boldsymbol{k}\cdot\boldsymbol{x}}\,|\psi\rangle, \tag{4.1}$$

where relevant definitions of the symbols can be found in Eqs. (2.18)–(2.21), and the contour $C_{\rm H}$ is as shown in Fig. 1. The high-energy part consists of the following integration region for the virtual photon:

$$\omega\in(E_n-i\,\infty,E_n+i\,\infty)$$
$$z\in(-i\,\infty,i\,\infty). \tag{4.2}$$

The separation of the high-energy part into a subtraction term and a remainder is accomplished as in the middle-energy part [see Eq. (3.22)] by writing the full Dirac-Coulomb Green function G [Eq. (2.19)] as $G=G_{\rm A}+G_{\rm B}$. We define the high-energy subtraction term $F_{\rm HA}$ as the expression obtained upon substitution of the propagator $G_{\rm A}$ for G in Eq. (4.1), and a substitution of the propagator $G_{\rm B}$ for G in Eq. (4.1) leads to the high-energy remainder $F_{\rm HB}$ which is discussed in Sec. IV B. The subtraction term (including all divergent contributions) is generated by $G_{\rm A}$, the high-energy remainder term corresponds to $G_{\rm B}$. We have

$$\Delta E_{\rm HA}=-\lim_{\Lambda\to\infty} i\,e^2\int_{C_{\rm H}}\frac{d\omega}{2\pi}\int\frac{d^3\boldsymbol{k}}{(2\pi)^3}D_{\mu\nu}(k^2,\Lambda)\times\langle\psi|\,\alpha^\mu\,e^{i\,\boldsymbol{k}\cdot\boldsymbol{x}}\,G_{\rm A}(E_n-\omega)\,\alpha^\nu\,e^{-i\,\boldsymbol{k}\cdot\boldsymbol{x}}\,|\psi\rangle \tag{4.3}$$

and

$$\Delta E_{\rm HB}=-i\,e^2\int_{C_{\rm H}}\frac{d\omega}{2\pi}\int\frac{d\boldsymbol{k}}{(2\pi)^3}D_{\mu\nu}(k^2)\times\langle\psi|\,\alpha^\mu\,e^{i\,\boldsymbol{k}\cdot\boldsymbol{x}}\,G_{\rm B}(E_n-\omega)\,\alpha^\nu\,e^{-i\,\boldsymbol{k}\cdot\boldsymbol{x}}\,|\psi\rangle. \tag{4.4}$$

The contribution $\Delta E_{\rm HA}$ corresponding to $G_{\rm A}$ can be separated further into a term $\Delta E_{\rm HA}^{(1)}$, which contains all divergent contributions, and a term $\Delta E_{\rm HA}^{(2)}$, which contains contributions of lower order than $(Z\alpha)^4$, but is convergent as $\Lambda\to\infty$. This separation is described in detail in [47,50]. We have

$$\Delta E_{\rm HA}=\Delta E_{\rm HA}^{(1)}+\Delta E_{\rm HA}^{(2)}. \tag{4.5}$$

We obtain for $\Delta E_{\rm HA}^{(1)}$, which contains a logarithmic divergence as $\Lambda\to\infty$,

$$\Delta E_{\rm HA}^{(1)}=\frac{\alpha}{\pi}\left[\left(\frac{3}{4}\ln\Lambda^2-\frac{9}{8}\right)\langle\beta\rangle+\left(\frac{1}{2}\ln 2-\frac{17}{12}\right)\langle V\rangle+\frac{(Z\alpha)^4}{n^3}F_{\rm HA}^{(1)}(nl_j,Z\alpha)\right]. \tag{4.6}$$

For the contribution $F_{\rm HA}^{(1)}$, an explicit analytic result is given in Eq. (4.15) in [47]. This contribution is therefore not discussed in any further detail here. The contribution $\Delta E_{\rm HA}^{(2)}$ contains lower-order terms,

$$\Delta E_{\rm HA}^{(2)}=\frac{\alpha}{\pi}\left[\left(-\frac{1}{2}\ln 2+\frac{1}{4}\right)\langle V\rangle+\frac{(Z\alpha)^4}{n^3}F_{\rm HA}^{(2)}(nl_j,Z\alpha)\right]. \tag{4.7}$$

Altogether we have

$$\Delta E_{\rm HA}=\Delta E_{\rm HA}^{(1)}+\Delta E_{\rm HA}^{(2)}=\frac{\alpha}{\pi}\left[\left(\frac{3}{4}\ln\Lambda^2-\frac{9}{8}\right)\langle\beta\rangle-\frac{7}{6}\langle V\rangle+\frac{(Z\alpha)^4}{n^3}F_{\rm HA}(nl_j,Z\alpha)\right]. \tag{4.8}$$

The scaled function $F_{\rm HA}(nl_j,Z\alpha)$ is given by

$$F_{\rm HA}(nl_j,Z\alpha)=F_{\rm HA}^{(1)}(nl_j,Z\alpha)+F_{\rm HA}^{(2)}(nl_j,Z\alpha). \tag{4.9}$$

The term $\Delta E_{\rm HA}^{(2)}$ falls naturally into a sum of four contributions [47],

$$\Delta E_{\rm HA}^{(2)}=T_1+T_2+T_3+T_4, \tag{4.10}$$

where

$$T_1=-\frac{1}{10}\langle V\rangle+\frac{(Z\alpha)^4}{n^3}h_1(nl_j,Z\alpha),$$

TABLE IV. Numerical results for the high-energy subtraction term $F_{\rm HA}$ and the high-energy remainder term $F_{\rm HB}$. The high-energy term $F_{\rm H}$ is the sum $F_{\rm H}(nl_j,Z\alpha)=F_{\rm HA}(nl_j,Z\alpha)+F_{\rm HB}(nl_j,Z\alpha)$.

Z	$F_{\rm HA}(1S_{1/2},Z\alpha)$	$F_{\rm HA}(2S_{1/2},Z\alpha)$	$F_{\rm HA}(2P_{1/2},Z\alpha)$	$F_{\rm HA}(2P_{3/2},Z\alpha)$
1	−1.216 846 660 6(1)	−1.420 293 291(1)	−1.081 265 954(1)	−0.524 359 802(1)
2	−1.214 322 536 9(1)	−1.417 829 864(1)	−1.081 451 269(1)	−0.524 385 053(1)
3	−1.212 026 714 1(1)	−1.415 635 310(1)	−1.081 760 224(1)	−0.524 427 051(1)
4	−1.209 942 847 4(1)	−1.413 693 422(1)	−1.082 192 995(1)	−0.524 485 727(1)
5	−1.208 059 033 6(1)	−1.411 992 480(1)	−1.082 749 845(1)	−0.524 561 017(1)
Z	$F_{\rm HB}(1S_{1/2},Z\alpha)$	$F_{\rm HB}(2S_{1/2},Z\alpha)$	$F_{\rm HB}(2P_{1/2},Z\alpha)$	$F_{\rm HB}(2P_{3/2},Z\alpha)$
1	−0.088 357 254(1)	−0.018 280 727(5)[a]	0.014 546 64(1)	−0.042 310 69(1)
2	−0.082 758 206(1)	−0.012 729 99(1)	0.014 574 21(1)	−0.042 296 81(1)
3	−0.076 811 229(1)	−0.006 861 02(1)	0.014 620 51(1)	−0.042 273 58(1)
4	−0.070 590 991(1)	−0.000 746 40(1)	0.014 685 82(1)	−0.042 240 92(1)
5	−0.064 146 139(1)	0.005 567 16(1)	0.014 770 52(1)	−0.042 198 76(1)
Z	$F_{\rm H}(1S_{1/2},Z\alpha)$	$F_{\rm H}(2S_{1/2},Z\alpha)$	$F_{\rm H}(2P_{1/2},Z\alpha)$	$F_{\rm H}(2P_{3/2},Z\alpha)$
1	−1.305 203 915(1)	−1.438 574 018(5)	−1.066 719 31(1)	−0.566 670 50(1)
2	−1.297 080 743(1)	−1.430 559 85(1)	−1.066 877 06(1)	−0.566 681 86(1)
3	−1.288 837 943(1)	−1.422 496 33(1)	−1.067 139 72(1)	−0.566 700 63(1)
4	−1.280 533 839(1)	−1.414 439 82(1)	−1.067 507 18(1)	−0.566 726 65(1)
5	−1.272 205 173(1)	−1.406 425 32(1)	−1.067 979 33(1)	−0.566 759 78(1)

[a]Result obtained with a greater number of integration nodes than are used for the higher-Z results.

$$T_2=\left(\frac{7}{20}-\frac{1}{2}\ln 2\right)\langle V\rangle+\frac{(Z\alpha)^4}{n^3}h_2(nl_j,Z\alpha),$$

$$T_3=\frac{(Z\alpha)^4}{n^3}h_3(nl_j,Z\alpha),$$

$$T_4=\frac{(Z\alpha)^4}{n^3}h_4(nl_j,Z\alpha). \tag{4.11}$$

The functions h_i $(i=1,2,3,4)$ are defined in Eqs. (4.18), (4.19), and (4.21) in [47] (see also Eq. (3.6) in [49]). The evaluation of the high-energy subtraction term proceeds as outlined in [47–49], albeit with an increased accuracy and improved calculational methods in intermediate steps of the calculation in order to overcome the severe numerical cancellations in the low-Z region. We recover $F^{(2)}_{\rm HA}$ as the sum

$$F^{(2)}_{\rm HA}(nl_j,Z\alpha)=h_1(nl_j,Z\alpha)+h_2(nl_j,Z\alpha)+h_3(nl_j,Z\alpha)+h_4(nl_j,Z\alpha). \tag{4.12}$$

The scaled function $F_{\rm HA}(nl_j,Z\alpha)$ [see also Eqs. (2.26) and (2.28)] is given by

$$F_{\rm HA}(nl_j,Z\alpha)=F^{(1)}_{\rm HA}(nl_j,Z\alpha)+F^{(2)}_{\rm HA}(nl_j,Z\alpha). \tag{4.13}$$

The limits of the contributions $F^{(1)}_{\rm HA}(nl_j,Z\alpha)$ and $F^{(2)}_{\rm HA}(nl_j,Z\alpha)$ as $(Z\alpha)\to 0$ have been investigated in [47,49,50]. For the contribution $F^{(1)}_{\rm HA}(nl_j,0)$, the result can be found in Eq. (3.5) in [49]. The limits of the functions $h_i(nl_j,Z\alpha)$ $(i=1,2,3,4)$ as $Z\alpha\to 0$ are given as a function of the atomic state quantum numbers in Eq. (3.8) in [49]. For the scaled high-energy subtraction term $F_{\rm HA}$, the limits read [see Eq. (3.9) in [49]]

$$F_{\rm HA}(nl_j,Z\alpha)=\left(\frac{11}{10}-\ln 2\right)\frac{1}{n}+\left(\frac{16}{15}-2\ln 2\right)\frac{1}{2l+1}+\left(\frac{1}{2}\ln 2-\frac{1}{4}\right)\frac{1}{\kappa(2l+1)}+\left(\frac{3}{2}\ln 2-\frac{9}{4}\right)\frac{1}{|\kappa|}+O(Z\alpha). \tag{4.14}$$

Therefore, the explicit forms of the limits for the states under investigation in this paper are

$$\begin{aligned}
F_{\rm HA}(1S_{1/2},Z\alpha)&=-1.219\,628+O(Z\alpha),\\
F_{\rm HA}(2S_{1/2},Z\alpha)&=-1.423\,054+O(Z\alpha),\\
F_{\rm HA}(2P_{1/2},Z\alpha)&=-1.081\,204+O(Z\alpha),\\
F_{\rm HA}(2P_{3/2},Z\alpha)&=-0.524\,351+O(Z\alpha).
\end{aligned} \tag{4.15}$$

Numerical results for $F_{\rm HA}$, which are presented in Table IV, exhibit consistency with the limits in Eq. (4.15).

B. The high-energy remainder

The remainder term in the high-energy part involves the propagator $G_{\rm B}$ defined in Eq. (2.39), $G_{\rm B}=G-G_{\rm A}$, where G is defined in Eq. (2.19) and $G_{\rm A}$ is given in Eq. (2.38). The energy shift is

$$\Delta E_{\rm HB} = -\frac{i\,\alpha}{\pi}\int_0^{i\,\infty} dz \int_0^{\infty} dx_1\, x_1^2 \int_0^{x_1} dx_2\, x_2^2 \times\{\mathcal{M}_{\rm HB}(x_2,x_1,z)+{\rm c.c.}\}, \tag{4.16}$$

where c.c. denotes the complex conjugate. The photon energy integration is evaluated with the aid of the substitution

$$z\to i\,u \quad \text{where} \quad u=\frac{1}{2}\left(\frac{1}{t}-t\right). \tag{4.17}$$

In analogy with the middle-energy subtraction and remainder terms discussed in Secs. III B and III C [see especially Eqs. (3.26) and (3.31)], the functions $\mathcal{M}_{\rm HB}(x_2,x_1,z)$ and $S_{\rm HB}(r,y,z)$ and the terms $T_{{\rm HB},|\kappa|}$ are defined implicitly in the following:

$$\begin{aligned} S_{\rm HB}(r,y,t) &= \left(1+\frac{1}{t^2}\right)\frac{r^2y^5}{a^6}{\rm Re}\left[\mathcal{M}_{\rm HB}\left(\frac{r\,y}{a},\frac{y}{a},i\,u\right)\right] \\ &= \left(1+\frac{1}{t^2}\right)\frac{r^2y^5}{a^6}\sum_{|\kappa|=1}^{\infty}\sum_{\kappa=\pm|\kappa|}\sum_{i,j=1}^{2}{\rm Re}\Bigg[f_i\left(\frac{r\,y}{a}\right) \\ &\quad\times G^{ij}_{{\rm B},\kappa}\left(\frac{r\,y}{a},\frac{y}{a},i\,u\right) f_j\left(\frac{y}{a}\right)\mathcal{A}_\kappa\left(\frac{r\,y}{a},\frac{y}{a}\right) \\ &\quad - f_{\bar\imath}\left(\frac{r\,y}{a}\right) G^{ij}_{{\rm B},\kappa}\left(\frac{r\,y}{a},\frac{y}{a},i\,u\right) \\ &\quad\times f_{\bar\jmath}\left(\frac{y}{a}\right)\mathcal{A}^{ij}_\kappa\left(\frac{r\,y}{a},\frac{y}{a}\right)\Bigg] \\ &= \left(1+\frac{1}{t^2}\right)\frac{r^2y^5}{a^6}\sum_{|\kappa|=1}^{\infty} T_{{\rm HB},|\kappa|}(r,y,t). \end{aligned} \tag{4.18}$$

The only substantial difference from the treatment of the middle-energy remainder lies in the prefactor generated by the parametrization of the complex photon energy given in Eq. (4.17). The photon angular functions $\mathcal{A}_\kappa$ and $\mathcal{A}^{ij}_\kappa$ $(i,j=1,2)$ *for the high-energy part* are defined in Eq. (5.8) of Ref. [47] and in Eq. (4.3) in [49] for an arbitrary bound state. Special formulas for the ground state can be found in Eq. (5.9) of Ref. [47]. The functions $\mathcal{A}_\kappa$ and $\mathcal{A}^{ij}_\kappa$ are *not* identical to the photon angular functions for the infrared and middle-energy parts A^{ij}_κ $(i,j=1,2)$ which are used for the low-energy part of the calculation in Sec. III. It might be worth mentioning that in [46–49] both the functions A^{ij}_κ and $\mathcal{A}^{ij}_\kappa$ are denoted by the symbol A^{ij}_κ. It is clear from the context which of the functions is employed in each case.

In the last line of Eq. (4.18), we implicitly define the terms $T_{{\rm HB},|\kappa|}$ as

$$\begin{aligned} T_{{\rm HB},|\kappa|}(r,y,t) &= \sum_{\kappa=\pm|\kappa|}\sum_{i,j=1}^{2}{\rm Re}\Bigg[f_i\left(\frac{r\,y}{a}\right)G^{ij}_{{\rm B},\kappa}\left(\frac{r\,y}{a},\frac{y}{a},i\,u\right) \\ &\quad\times f_j\left(\frac{y}{a}\right)\mathcal{A}_\kappa\left(\frac{r\,y}{a},\frac{y}{a}\right) - f_{\bar\imath}\left(\frac{r\,y}{a}\right) \\ &\quad\times G^{ij}_{{\rm B},\kappa}\left(\frac{r\,y}{a},\frac{y}{a},i\,u\right) f_{\bar\jmath}\left(\frac{y}{a}\right)\mathcal{A}^{ij}_\kappa\left(\frac{r\,y}{a},\frac{y}{a}\right)\Bigg]. \end{aligned} \tag{4.19}$$

With these definitions, the high-energy remainder can be rewritten as

$$\Delta E_{\rm HB}=\frac{\alpha}{\pi}\int_0^1 dt\int_0^1 dr\int_0^{\infty} dy\, S_{\rm HB}(r,y,t). \tag{4.20}$$

There are no lower-order terms to subtract, and therefore

$$\Delta E_{\rm HB}=\frac{\alpha}{\pi}\frac{(Z\alpha)^4}{n^3}F_{\rm HB}(nl_j,Z\alpha). \tag{4.21}$$

For the high-energy remainder $F_{\rm HB}$, the limits as $Z\alpha\to 0$ read [see Eq. (4.15) in [49]]

$$F_{\rm HB}(nl_j,Z\alpha)=\frac{1}{2\,l+1}\left[\left(\frac{17}{18}-\frac{4}{3}\ln 2\right)\delta_{l,0}+\left(\frac{3}{2}-2\ln 2\right)\frac{1}{\kappa} +\left(\frac{5}{6}-\ln 2\right)\frac{n-2\,l-1}{n}\right]+O(Z\alpha). \tag{4.22}$$

For the atomic states under investigation, this leads to

$$\begin{aligned} F_{\rm HB}(1S_{1/2},Z\alpha) &= -0.093\,457+O(Z\alpha),\\ F_{\rm HB}(2S_{1/2},Z\alpha) &= -0.023\,364+O(Z\alpha),\\ F_{\rm HB}(2P_{1/2},Z\alpha) &= 0.014\,538+O(Z\alpha),\\ F_{\rm HB}(2P_{3/2},Z\alpha) &= -0.042\,315+O(Z\alpha). \end{aligned} \tag{4.23}$$

The integration procedure for the high-energy part is adapted to the problem at hand. To this end, a crude estimate is found for the dependence of the function $S_{\rm HB}$ defined in Eq. (4.18) on its arguments. The considerations leading to this estimate are analogous to those outlined in Sec. III A for the infrared part. The result is the approximate expression

$$e^{-y}\exp\left[-\left(\frac{1}{a\,t}-\frac{1}{2}\right)(1-r)\,y\right] \tag{4.24}$$

for $S_{\rm HB}$. This leads naturally to the definition

$$q_{\rm HB}=1+\left(\frac{1}{a\,t}-\frac{1}{2}\right)(1-r), \tag{4.25}$$

so that the (approximate) dependence of $S_{\rm HB}$ on the radial variable at large y is $\exp(-q_{\rm HB}y)$. Note that $q_{\rm HB}$ may assume large values ($\gg 1$) as $t\to 0$; this is unlike the analogous quantity

$$1+\left(\frac{c}{a}-\frac{1}{2}\right)(1-r)$$

in the infrared and the middle-energy part, where $|c| = |\sqrt{1-z^2}|<1$ because $z\in(0,E_n)$. Having identified the leading exponential asymptotic behavior of the integrand $S_{\rm HB}$, it is rather straightforward to evaluate the three-dimensional integral in Eq. (4.20) by Gauss-Laguerre and Gauss-Legendre quadrature [5] [the scaling parameter a is defined in Eqs. (3.9) and (3.14)]. The numerical results for the high-energy remainder function $F_{\rm HB}$ are found in Table IV. These results are consistent with the limits in Eq. (4.23).

We now turn to a brief discussion of the convergence acceleration techniques used in the evaluation of the function $S_{\rm HB}$ defined in Eq. (4.18). The angular momentum decomposition of $S_{\rm HB}$ gives rise to a sum over the terms $T_{{\rm HB},|\kappa|}$ [see the last line of Eq. (4.18)], where $|\kappa|$ represents the modulus of the Dirac angular momentum quantum number of the virtual intermediate state. In shorthand notation, and suppressing the arguments, we have

$$S_{\rm HB}\propto\sum_{|\kappa|=1}^{\infty} T_{{\rm HB},|\kappa|}\,. \tag{4.26}$$

The radial Green function $G_{\rm B}=G_{\rm B}(ry/a,y/a,z)$ in coordinate space needs to be evaluated at the radial arguments $r\,y/a$ and y/a (where $0<r<1$), and at the energy argument $z=E_n-\omega=i/2\,(t^{-1}-t)$ [see Eq. (4.18)]. A crucial role is played by the ratio r of the two radial arguments. Indeed, for $|\kappa|\to\infty$, we have [see Eq. (4.7) in [48]]

$$T_{{\rm HB},|\kappa|}=\frac{r^{2\,|\kappa|}}{|\kappa|}\left[\text{const}+O\left(\frac{1}{|\kappa|}\right)\right], \tag{4.27}$$

where ''const'' is independent of $|\kappa|$ and depends only on r, y, and t. The series in Eq. (4.26) is slowly convergent for r close to one, and the region near $r=1$ is known to be problematic in numerical evaluations. Additionally, note that the region at $r=1$ is more important at low Z than at high Z. This is because the function $S_{\rm HB}$, for constant y, depends on r roughly as $\exp[-y\,(1-r)/(a\,t)]$ [see Eq. (4.24)], where $a=2\,(Z\alpha)/n+O[(Z\alpha)^3]$. For small Z, the Bohr radius $1/(Z\alpha)$ of the hydrogenlike system is large compared to high-Z systems, which emphasizes the region near $r=1$. In this region the series in Eq. (4.26) is very slowly convergent. We have found that the convergence of this series near $r=1$ can be accelerated very efficiently using the combined nonlinear-condensation transformation [10] applied to the series $\Sigma_{k=0}^{\infty}t_k$ where $t_k=T_{{\rm HB},k+1}$ [see Eqs. (4.26) and (4.27)].

We first transform this series into an alternating series by a condensation transformation due to Van Wijngaarden [55,56],

$$\sum_{k=0}^{\infty} t_k=\sum_{j=0}^{\infty}(-1)^j\,\mathbf{A}_j\,, \tag{4.28}$$

where

$$\mathbf{A}_j=\sum_{k=0}^{\infty}2^k\,t_{2^k\,(j+1)-1}\,. \tag{4.29}$$

We then accelerate the convergence of the alternating series $\Sigma_{j=0}^{\infty}(-1)^j\,\mathbf{A}_j$ by applying the nonlinear delta transform $\delta_n^{(0)}(1,\mathbf{S}_0)$, which is discussed extensively in [57]. The explicit formula for this transformation is given by defining

$$\mathbf{S}_n=\sum_{j=0}^{n}(-1)^j\,\mathbf{A}_j \tag{4.30}$$

as the nth partial sum of the Van Wijngaarden transformed input series. The δ transform reads [see Eq. (8.4-4) of [57]],

$$\delta_n^{(0)}(1,\mathbf{S}_0)=\frac{\displaystyle\sum_{j=0}^{n}(-1)^j\binom{n}{j}\frac{(1+j)_{n-1}}{(1+n)_{n-1}}\frac{\mathbf{S}_j}{\mathbf{B}_{j+1}}}{\displaystyle\sum_{j=0}^{n}(-1)^j\binom{n}{j}\frac{(1+j)_{n-1}}{(1+n)_{n-1}}\frac{1}{\mathbf{B}_{j+1}}}, \tag{4.31}$$

where

$$\mathbf{B}_j=(-1)^j\,\mathbf{A}_j\,. \tag{4.32}$$

The convergence acceleration proceeds by calculating a sequence of transforms $\delta_n^{(0)}$ in increasing transformation order n. It is observed that the transforms converge much faster than the partial sums $\mathbf{S}_n$ defined in Eq. (4.30). The upper index zero in Eq. (4.31) indicates that the transformation is started with the first term $\mathbf{A}_0$.

The combined transformation (combination of the condensation transformation and the Weniger transformation) was found to be applicable to a wide range of slowly convergent monotone series (series whose terms have the same sign), and many examples for its application were given in Ref. [10]. For the numerical treatment of radiative corrections in low-Z systems, the transformation has the advantage of removing the principal numerical difficulties associated with the slow convergence of angular momentum decompositions of the propagators near their singularity for equal radial arguments.

In a typical case, sufficient precision (10^{-11}) in the convergence of the sum in Eq. (4.26) is reached in a transformation order $n<100$ for the nonlinear transformation $\delta_n^{(0)}(1,\mathbf{S}_0)$, a region in which the nonlinear sequence transformation δ is numerically stable. Although the δ transformation exhibits considerable numerical stability in higher transformation orders [10,57], inevitable round-off errors start to accumulate significantly in an excessively high transformation order of $n\approx500$ in a typical case [5], and this situation is avoided in the current evaluation because the transforms exhibit apparent convergence to the required accuracy before numerical round-off errors accumulate. Note that evaluation of the condensed series $\mathbf{A}_j$ in Eq. (4.29) entails sampling of terms $T_{{\rm HB},|\kappa|}$ for rather large $|\kappa|$, while eliminating the necessity of evaluating *all* terms $T_{{\rm HB},|\kappa|}$ up to the maximum index. The highest angular momentum $|\kappa|$ encountered in the present calculation is in excess of 4 000 000.

TABLE V. Numerical results for the scaled self-energy function F and the self-energy remainder function $G_{\rm SE}$.

Z	$F(1S_{1/2},Z\alpha)$	$F(2S_{1/2},Z\alpha)$	$F(2P_{1/2},Z\alpha)$	$F(2P_{3/2},Z\alpha)$
1	10.316 793 650(1)	10.546 825 185(5)	−0.126 396 37(1)	0.123 498 56(1)
2	8.528 325 052(1)	8.758 870 25(1)	−0.125 816 16(1)	0.123 835 55(1)
3	7.504 503 422(1)	7.735 777 20(1)	−0.124 992 24(1)	0.124 317 10(1)
4	6.792 824 081(1)	7.025 002 41(1)	−0.123 968 79(1)	0.124 918 48(1)
5	6.251 627 078(1)	6.484 860 42(1)	−0.122 774 94(1)	0.125 623 30(1)
Z	$G_{\rm SE}(1S_{1/2},Z\alpha)$	$G_{\rm SE}(2S_{1/2},Z\alpha)$	$G_{\rm SE}(2P_{1/2},Z\alpha)$	$G_{\rm SE}(2P_{3/2},Z\alpha)$
1	−30.290 24(2)	−31.185 15(9)	−0.9735(2)	−0.4865(2)
2	−29.770 967(5)	−30.644 66(5)	−0.949 40(5)	−0.470 94(5)
3	−29.299 170(2)	−30.151 93(2)	−0.926 37(2)	−0.456 65(2)
4	−28.859 222(1)	−29.691 27(1)	−0.904 12(1)	−0.443 13(1)
5	−28.443 372 3(8)[a]	−29.255 033(8)	−0.882 478(8)	−0.430 244(8)

[a]The result for this entry given in [4] contains a typographical error.

However, even in extreme cases less than 3000 evaluations of particular terms of the original series are required. The computer time for the evaluation of the slowly convergent angular-momentum expansion near the singularity is reduced by roughly three orders of magnitude by the use of the convergence acceleration methods.

In certain parameter regions (e.g., for large energy of the virtual photon), a number of terms of the input series t_k have to be skipped before the convergence acceleration algorithm defined in Eqs. (4.28)–(4.32) can be applied (in order to avoid transient behavior of the first few terms in the sum over κ). In this case, the input data for the combined nonlinear-condensation transformation are the terms $t_k = T_{\rm HB,k+1+\kappa_s}$, where κ_s denotes the number of terms that are directly summed before the transformation is applied. These issues and further details regarding the application of the convergence acceleration method to QED calculations can be found in Appendix H.2 of [5].

C. Results for the high-energy part

The limit of the function $F_{\rm H}$ as $Z\alpha\to 0$ can be derived easily from Eqs. (4.14) and (4.22) as a function of the bound-state quantum numbers. For $F_{\rm H}$ the limit is

$$F_{\rm H}(nl_j,Z\alpha)=\left(\frac{11}{10}-\ln 2\right)\frac{1}{n}+\left(\frac{16}{15}-2\,\ln 2\right)\frac{1}{2\,l+1}+\left(-\frac{3}{2}\ln 2+\frac{5}{4}\right)\frac{1}{\kappa\,(2\,l+1)}+\left(\frac{3}{2}\ln 2-\frac{9}{4}\right)\frac{1}{|\kappa|}+\left(\frac{17}{18}-\frac{4}{3}\ln 2\right)\delta_{l,0}+\left(\frac{5}{6}-\ln 2\right)\frac{n-2\,l-1}{n\,(2\,l+1)}+O(Z\alpha). \quad (4.33)$$

For the atomic states investigated here, this expression yields the numerical values

$$F_{\rm H}(1S_{1/2},Z\alpha)=-1.313\,085+O(Z\alpha),$$

$$F_{\rm H}(2S_{1/2},Z\alpha)=-1.446\,418+O(Z\alpha),$$

$$F_{\rm H}(2P_{1/2},Z\alpha)=-1.066\,667+O(Z\alpha),$$

$$F_{\rm H}(2P_{3/2},Z\alpha)=-0.566\,667+O(Z\alpha). \quad (4.34)$$

Numerical results for the high-energy part

$$F_{\rm H}(nl_j,Z\alpha)=F_{\rm HA}(nl_j,Z\alpha)+F_{\rm HB}(nl_j,Z\alpha) \quad (4.35)$$

are also summarized in Table IV. Note the apparent consistency of the numerical results in Table IV with their analytically obtained low-Z limits in Eq. (4.34).

V. COMPARISON TO ANALYTIC CALCULATIONS

The numerical results for the scaled self-energy function $F(nl_j,Z\alpha)$ defined in Eq. (2.1) are given in Table V, together with the results for the nonperturbative self-energy remainder function $G_{\rm SE}(nl_j,Z\alpha)$, which is implicitly defined in Eq. (2.2). Results are provided for K- and L-shell states. The results here at $Z=5$ are consistent with and much more precise than the best previous calculation [46]. The numerical results for the self-energy remainder $G_{\rm SE}$ are obtained by subtracting the analytic lower-order terms listed in Eq. (2.2) from the complete numerical result for the scaled self-energy function $F(nl_j,Z\alpha)$. No additional fitting is performed.

Analytic and numerical results at low Z can be compared by considering the self-energy remainder function $G_{\rm SE}$. Note that an inconsistency in any of the analytically obtained lower-order terms would be likely to manifest itself in a grossly inconsistent dependence of $G_{\rm SE}(nl_j,Z\alpha)$ on its argument $Z\alpha$; this is not observed. For S states, the following analytic model for $G_{\rm SE}$ is commonly assumed, which is motivated in part by a renormalization-group analysis [58] and is constructed in analogy with the pattern of the analytic coefficients A_{ij} in Eqs. (2.2) and (2.3),

$$G_{\rm SE}(nS_{1/2},Z\alpha)=A_{60}(nS_{1/2})+(Z\alpha)\,[A_{71}(nS_{1/2})\,\ln(Z\alpha)^{-2}+A_{70}(nS_{1/2})]+(Z\alpha)^2\,[A_{83}(nS_{1/2})\times\ln^3(Z\alpha)^{-2}+A_{82}(nS_{1/2})\,\ln^2(Z\alpha)^{-2}+A_{81}(nS_{1/2})\,\ln(Z\alpha)^{-2}+A_{80}(nS_{1/2})]. \tag{5.1}$$

The (probably nonvanishing) A_{83} coefficient, which introduces a triple logarithmic singularity at $Z\alpha=0$, hinders an accurate comparison of numerical and analytic data for $G_{\rm SE}$. A somewhat less singular behavior is expected of the difference

$$\Delta G_{\rm SE}(Z\alpha)=G_{\rm SE}(2S_{1/2},Z\alpha)-G_{\rm SE}(1S_{1/2},Z\alpha), \tag{5.2}$$

because the leading logarithmic coefficients in any given order of $Z\alpha$ are generally assumed to be equal for all S states, which would mean in particular

$$A_{71}(1S_{1/2})=A_{71}(2S_{1/2})$$

and

$$A_{83}(1S_{1/2})=A_{83}(2S_{1/2}). \tag{5.3}$$

Now we define ΔA_{kl} as the difference of the values of the analytic coefficients for the two lowest S states

$$\Delta A_{kl}=A_{kl}(2S_{1/2})-A_{kl}(1S_{1/2}). \tag{5.4}$$

The function $\Delta G_{\rm SE}$ defined in Eq. (5.2) can be assumed to have the following semi-analytic expansion about $Z\alpha=0$:

$$\Delta G_{\rm SE}(Z\alpha)=\Delta A_{60}+(Z\alpha)\,\Delta A_{70}+(Z\alpha)^2\,[\Delta A_{82}\ln^2(Z\alpha)^{-2}+\Delta A_{81}\ln(Z\alpha)^{-2}+\Delta A_{80}+o(Z\alpha)]. \tag{5.5}$$

In order to detect possible inconsistencies in the numerical and analytic data for $G_{\rm SE}$, we difference the data for $\Delta G_{\rm SE}$, i.e., we consider the following finite difference approximation to the derivative of the function $\Delta G_{\rm SE}$:

$$g(Z)=\Delta G_{\rm SE}((Z+1)\,\alpha)-\Delta G_{\rm SE}(Z\alpha). \tag{5.6}$$

We denote the analytic and numerical limits of $\Delta G_{\rm SE}(Z\alpha)$ as $Z\alpha\to0$ as $\Delta A_{60}^{(\rm an)}$ and $\Delta A_{60}^{(\rm nu)}$, respectively, and leave open the possibility of an inconsistency between numerical and analytic data by keeping $\Delta A_{60}^{(\rm nu)}$ and $\Delta A_{60}^{(\rm an)}$ as distinct variables. In order to illustrate how a discrepancy could be detected by investigating the function $g(Z)$, we consider special cases of the function $\Delta G_{\rm SE}(Z\alpha)$ and $g(Z)$. We have for $Z=0$, which is determined exclusively by analytic results,

$$\Delta G_{\rm SE}(0)=\Delta A_{60}^{(\rm an)}, \tag{5.7}$$

whereas for $Z=1$, which is determined by numerical data,

$$\Delta G_{\rm SE}(\alpha)=\Delta A_{60}^{(\rm nu)}+\alpha\,[\Delta A_{70}+o(\alpha)], \tag{5.8}$$

and for $Z=2$,

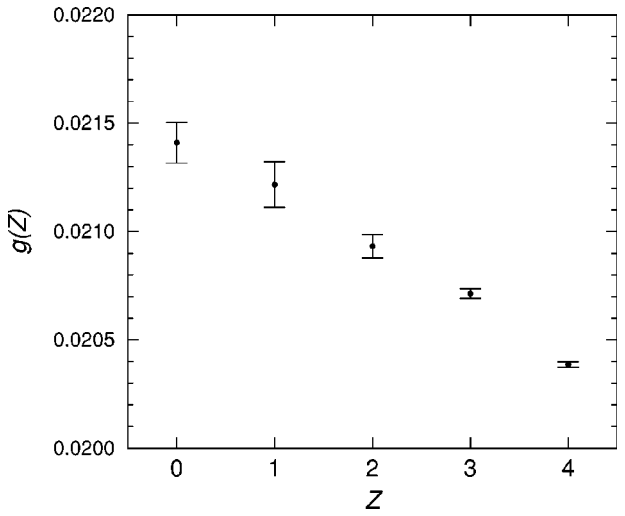

FIG. 4. Plot of the function $g(Z)$ defined in Eq. (5.6) in the region of low nuclear charge. For the evaluation of the data point at $Z=0$, a value of $A_{60}(1S_{1/2})=-30.924\,15(1)$ is employed [4,15,59].

$$\Delta G_{\rm SE}(2\alpha)=\Delta A_{60}^{(\rm nu)}+\alpha\,[2\,\Delta A_{70}+o(\alpha)], \tag{5.9}$$

etc. Hence for $Z=0$, we have

$$g(0)=\Delta G_{\rm SE}(\alpha)-\Delta G_{\rm SE}(0)=\Delta A_{60}^{(\rm nu)}-\Delta A_{60}^{(\rm an)}+\alpha\,[\Delta A_{70}+o(Z\alpha)]. \tag{5.10}$$

For $Z=1$, the value of g is determined solely by numerical data,

$$g(1)=\Delta G_{\rm SE}(2\alpha)-\Delta G_{\rm SE}(\alpha)=\alpha\,[\Delta A_{70}+o(Z\alpha)], \tag{5.11}$$

and for $Z=2$, we have

$$g(2)=\Delta G_{\rm SE}(3\alpha)-\Delta G_{\rm SE}(2\alpha)=\alpha\,[\Delta A_{70}+o(Z\alpha)]. \tag{5.12}$$

Analogous equations hold for $Z>2$. The analytic data and the numerical data from Table V lead to the five values $g(0)$, $g(1)$, $g(2)$, $g(3)$, and $g(4)$. A plot of the function $g(Z)$ serves two purposes: First, the values $g(1),\ldots,g(4)$ should exhibit apparent convergence to some limiting value $\alpha\,\Delta A_{70}$ as $Z\to0$, and this can be verified by inspection of the plot. Second, a discrepancy between the analytic and numerical approaches would result in a nonvanishing value for $\Delta A_{60}^{(\rm nu)}-\Delta A_{60}^{(\rm an)}$ which would appear as an inconsistency between the trend in the values of $g(1),\ldots,$ and $g(4)$ and the value of $g(0)$ [see Eq. (5.10)].

Among the separate evaluations of A_{60} for the ground state, the result in [15] has the smallest quoted uncertainty. In Fig. 4 we display a plot of $g(Z)$ for low nuclear charge Z. A value of $A_{60}(1S_{1/2})=A_{60}^{(\rm an)}(1S_{1/2})=-30.924\,15(1)$ [4,15,59] is used in Fig. 4. The results indicate very good agreement between the numerical and analytic approaches to the Lamb shift in the low-Z region up to the level of a few Hz in frequency units for the low-lying atomic states (where

n is the principal quantum number). The error bars represent the numerical uncertainty of the values in Table V, which correspond to an uncertainty on the level of $1.0\times Z^4$ Hz in frequency units.

Analytic work on the correction A_{60} has extended over three decades [15,34–37]. The complication arises that although the calculations are in general analytic, some remaining one-dimensional integrations could not be evaluated analytically because of the nature of the integrands [see, e.g., Eq. (6.96) in [15]]. Therefore a step-by-step comparison of the analytic calculations is difficult. An additional difficulty is the isolation of those analytic terms which contribute in a given order in $Z\alpha$, i.e., the isolation of only those terms which contribute to A_{60}. The apparent consistency of the numerical and analytic data in Fig. 4 represents an independent consistency check on the rather involved analytic calculations.

Our numerical results are not inconsistent with the analytic result [6] for a higher-order logarithm,

$$A_{71}=\pi\,(\tfrac{139}{64}-\ln 2)=4.65, \tag{5.13}$$

although they do not necessarily confirm it. As in [4], we obtain as an estimate $A_{71}=5.5(1.0)$ (from the fit to the numerical data for both S states). Logarithmic terms corresponding to the (probably) nonvanishing A_{83} coefficient should be taken into account for a consistent fit of the corrections to $G_{\rm SE}$. These highly singular terms are difficult to handle with a numerical fitting procedure. The terms A_{83}, A_{82}, and A_{81} furnish three more free parameters for the numerical fit, where only five data points are available (in addition to the quantities A_{60}, A_{71}, and A_{70}, which may also be regarded as free parameters for the fitting procedure). The determination of A_{60} by a fit from the numerical data is much more stable than the determination of the logarithmic correction A_{71}. We briefly note that our all-order evaluation essentially eliminates the uncertainty due to the unknown higher-order analytic terms. Also, it is interesting to note that the same numerical methods are employed for both the S and P states in our all-order (in $Z\alpha$) calculation, whereas the analytic treatment of S and P states differs [15,16].

The comparison of numerical and analytic results is much less problematic for P states, because the function $G_{\rm SE}$ is less singular [see Eqs. (2.4) and (2.6)]. For the $2P$ states, we observe that the function $G_{\rm SE}(2P_j,Z\alpha)$ has the same semi-analytic expansion about $Z\alpha=0$ as the function $\Delta G_{\rm SE}(Z\alpha)$ defined for S states in Eq. (5.2). We have

$$\begin{aligned} G_{\rm SE}(2P_j,Z\alpha)=&A_{60}(2P_j)+(Z\alpha)\,A_{70}(2P_j)+(Z\alpha)^2\\ &\times[A_{82}(2P_j)\ln^2(Z\alpha)^{-2}+A_{81}(2P_j)\\ &\times\ln(Z\alpha)^{-2}+A_{80}(2P_j)+o(Z\alpha)]. \end{aligned} \tag{5.14}$$

Hence, we plot the function

$$g_j(Z)=G_{\rm SE}(2P_j,(Z+1)\,\alpha)-G_{\rm SE}(2P_j,Z\alpha) \tag{5.15}$$

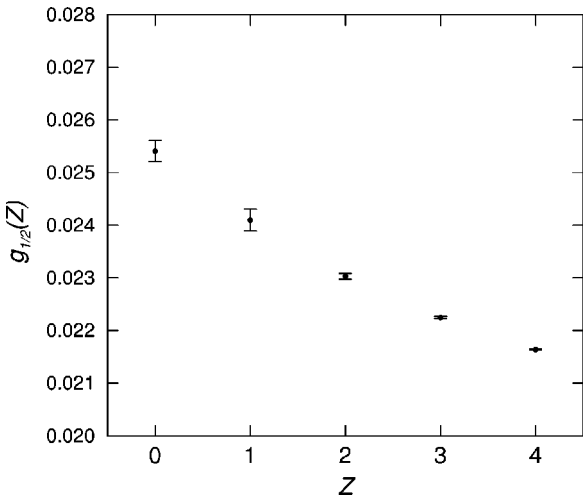

FIG. 5. Comparison of numerical data and analytically evaluated higher-order binding corrections for the $2P_{1/2}$ state. We plot the function $g_{1/2}(Z)$ defined in Eq. (5.15) in the region of low Z. The numerical data obtained in the current investigation appear to be consistent with the analytic result of $A_{60}(2P_{1/2})=-0.998\,91(1)$ obtained in [16].

for $j=\frac{1}{2}$ and $j=\frac{3}{2}$ in the region of low Z, with the notion that an inconsistent analytic result for $A_{60}(2P_j)$ would lead to irregularity at $Z=0$, in analogy with the S states. The numerical data shown in Figs. 5 and 6 appear to be consistent with the analytic results of

$$A_{60}(2P_{1/2})=-0.998\,91(1)$$

and

$$A_{60}(2P_{3/2})=-0.503\,37(1) \tag{5.16}$$

obtained in [16]. In this context it may be interesting to note that analytic results obtained in [16,52] for the higher-order binding corrections to $2P$, $3P$, and $4P$ states have recently

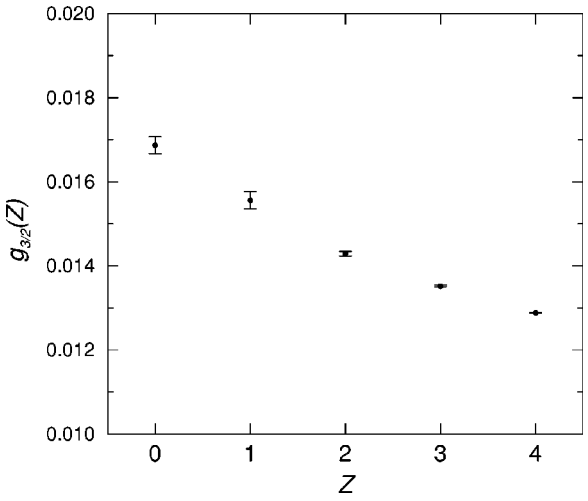

FIG. 6. For the $2P_{3/2}$ state, we plot the function $g_{3/2}(Z)$ defined in Eq. (5.15) in the region of low Z. The numerical data obtained in the current investigation appear to be consistent with the analytic result of $A_{60}(2P_{3/2})=-0.503\,37(1)$ from [16].

been confirmed indirectly [60]. Finally, although it may be possible to obtain more accurate estimates of some higher-order analytic corrections, notably the A_{70} coefficient for P states and ΔA_{70} for the two lowest-lying S states, we have not made such an analysis in the current work; we have restricted the discussion to a check of the consistency with the available results for A_{60}.

VI. CONCLUSION

There has recently been a rather broad interest in the numerical calculation of relativistic, QED self-energy, and two-body corrections at low Z and the comparison of analytic and numerical results [58,61–72]. Traditionally, the self-energy correction for hydrogenlike systems has posed a computational challenge. Here we have described a nonperturbative evaluation of the one-photon self-energy correction in hydrogenlike ions with low nuclear charge numbers $Z=1$ to 5. The general outline of our approach is discussed in Sec. II. In Sec. III the numerical evaluation of the low-energy part (generated by virtual photons of low energy) is described. In Sec. IV we discuss the numerical evaluation of the high-energy part, which is generated by high-energy virtual photons and contains the formally infinite contributions, which are removed by the renormalization. Section IV also contains a brief discussion of the convergence acceleration methods as employed in the current evaluation. We discuss in Sec. V the comparison of analytic and numerical data for K- and L-shell states in the region of low Z. The main results of this paper are contained in Table V: numerical data, nonperturbative in $Z\alpha$, for the scaled self-energy function F and the self-energy remainder function $G_{\rm SE}$ for K- and L-shell states at low nuclear charge. The numerical accuracy of our data is 1 Hz or better in frequency units for $1S$, $2S$, and both $2P$ states in atomic hydrogen.

The comparison of analytic and numerical results to the level of accuracy of the numerical data, which is discussed in Sec. V, indicates that there is very good agreement for the K- and L-shell states. The analytic and numerical data are shown in Figs. 4, 5, and 6. Our all-order evaluation eliminates any uncertainty due to the unknown higher-order analytic terms; the current numerical uncertainty in the self-energy is at the level of 1 Hz for atomic hydrogen.

ACKNOWLEDGMENTS

U. D. J. thanks the National Institute of Standards and Technology for kind hospitality during a number of extended research appointments. He would also like to acknowledge support from the Deutscher Akademischer Austauschdienst (DAAD). The authors would like to acknowledge helpful discussions with K. Pachucki, S. Karshenboim, and J. Sims. P. J. M. acknowledges the Alexander von Humboldt Foundation for continued support. The authors wish to acknowledge support from BMBF, DFG, and from GSI.

[1] B. de Beauvoir, F. Nez, L. Julien, B. Cagnac, F. Biraben, D. Touahri, L. Hilico, O. Acef, A. Clairon, and J. J. Zondy, Phys. Rev. Lett. **78**, 440 (1997).
[2] T. Udem, A. Huber, B. Gross, J. Reichert, M. Prevedelli, M. Weitz, and T. W. Hänsch, Phys. Rev. Lett. **79**, 2646 (1997).
[3] M. Niering, R. Holzwarth, J. Reichert, P. Pokasov, T. Udem, M. Weitz, T. W. Hänsch, P. Lemonde, G. Santarelli, M. Abgrall, P. Laurent, C. Salomon, and A. Clairon, Phys. Rev. Lett. **84**, 5496 (2000).
[4] U. D. Jentschura, P. J. Mohr, and G. Soff, Phys. Rev. Lett. **82**, 53 (1999).
[5] U. D. Jentschura, Ph.D. thesis, Technical University of Dresden [published as *Quantum Electrodynamic Radiative Corrections in Bound Systems, Dresdner Forschungen: Theoretische Physik, Band 2* (w.e.b. Universitätsverlag, Dresden, 1999).
[6] S. G. Karshenboim, Z. Phys. D: At., Mol. Clusters **39**, 109 (1997).
[7] T. W. Hänsch (private communication).
[8] C. L. Cesar, D. G. Fried, T. C. Killian, A. D. Polcyn, J. C. Sandberg, I. A. Yu, T. J. Greytak, D. Kleppner, and J. M. Doyle, Phys. Rev. Lett. **77**, 255 (1996).
[9] T. C. Killian, D. G. Fried, L. Willmann, D. Landhuis, S. C. Moss, T. J. Greytak, and D. Kleppner, Phys. Rev. Lett. **81**, 3807 (1998).
[10] U. D. Jentschura, P. J. Mohr, G. Soff, and E. J. Weniger, Comput. Phys. Commun. **116**, 28 (1999).
[11] W. R. Johnson and G. Soff, At. Data Nucl. Data Tables **33**, 405 (1985).
[12] P. J. Mohr, G. Plunien, and G. Soff, Phys. Rep. **293**, 227 (1998).
[13] P. J. Mohr, in *Atomic, Molecular, and Optical Physics Handbook*, edited by G. W. F. Drake (AIP, New York, 1996), pp. 341–351.
[14] M. I. Eides, H. Grotch, and V. A. Shelyuto, e-print hep-ph/0002158, Phys. Rep. (to be published).
[15] K. Pachucki, Ann. Phys. (N.Y.) **226**, 1 (1993).
[16] U. D. Jentschura and K. Pachucki, Phys. Rev. A **54**, 1853 (1996).
[17] E. T. Whittaker and G. N. Watson, *A Course of Modern Analysis* (Cambridge University Press, Cambridge, UK, 1944).
[18] H. Erdelyi, *Asymptotic Expansions* (Dover, New York, 1987).
[19] H. A. Bethe, Phys. Rev. **72**, 339 (1947).
[20] R. P. Feynman, Phys. Rev. **74**, 1430 (1948).
[21] R. P. Feynman, Phys. Rev. **76**, 769 (1949).
[22] J. B. French and V. F. Weisskopf, Phys. Rev. **75**, 1240 (1949).
[23] N. M. Kroll and W. E. Lamb, Phys. Rev. **75**, 388 (1949).
[24] J. Schwinger, Phys. Rev. **75**, 898 (1949).
[25] H. Fukuda, Y. Miyamoto, and S. Tomonaga, Prog. Theor. Phys. **4**, 47 (1949).
[26] M. Baranger, Phys. Rev. **84**, 866 (1951).
[27] R. Karplus, A. Klein, and J. Schwinger, Phys. Rev. **86**, 288 (1952).
[28] M. Baranger, H. A. Bethe, and R. P. Feynman, Phys. Rev. **92**, 482 (1953).
[29] H. M. Fried and D. R. Yennie, Phys. Rev. **112**, 1391 (1958).

[30] H. M. Fried and D. R. Yennie, Phys. Rev. Lett. **4**, 583 (1960).
[31] A. J. Layzer, Phys. Rev. Lett. **4**, 580 (1960).
[32] A. J. Layzer, J. Math. Phys. **2**, 292 (1961).
[33] A. J. Layzer, J. Math. Phys. **2**, 308 (1961).
[34] G. W. Erickson and D. R. Yennie, Ann. Phys. (N.Y.) **35**, 271 (1965).
[35] G. W. Erickson and D. R. Yennie, Ann. Phys. (N.Y.) **35**, 447 (1965).
[36] G. W. Erickson, Phys. Rev. Lett. **27**, 780 (1971).
[37] J. Sapirstein, Phys. Rev. Lett. **47**, 1723 (1981).
[38] S. Klarsfeld and A. Maquet, Phys. Lett. **43B**, 201 (1973).
[39] H. A. Bethe, L. M. Brown, and J. R. Stehn, Phys. Rev. **77**, 370 (1950).
[40] J. M. Harriman, Phys. Rev. **101**, 594 (1956).
[41] C. Schwartz and J. J. Tieman, Ann. Phys. (N.Y.) **6**, 178 (1959).
[42] M. Lieber, Phys. Rev. **174**, 2037 (1968).
[43] R. W. Huff, Phys. Rev. **186**, 1367 (1969).
[44] G. W. Erickson, J. Phys. Chem. Ref. Data **6**, 831 (1977).
[45] G. W. F. Drake and R. A. Swainson, Phys. Rev. A **41**, 1243 (1990).
[46] P. J. Mohr, Phys. Rev. A **46**, 4421 (1992).
[47] P. J. Mohr, Ann. Phys. (N.Y.) **88**, 26 (1974).
[48] P. J. Mohr, Ann. Phys. (N.Y.) **88**, 52 (1974).
[49] P. J. Mohr, Phys. Rev. A **26**, 2338 (1982).
[50] P. J. Mohr, Ph.D. thesis, University of California, Berkeley, 1973 (unpublished).
[51] P. J. Mohr and Y. K. Kim, Phys. Rev. A **45**, 2727 (1992).
[52] U. D. Jentschura, G. Soff, and P. J. Mohr, Phys. Rev. A **56**, 1739 (1997).
[53] P. J. Mohr and B. N. Taylor, Rev. Mod. Phys. **72**, 351 (2000)
[54] Certain commercial equipment, instruments, or materials are identified in this paper to foster understanding. Such identification does not imply recommendation or endorsement by the National Institute of Standards and Technology, nor does it imply that the materials or equipment identified are necessarily the best available for the purpose.
[55] C. W. Clenshaw, E. T. Goodwin, D. W. Martin, G. F. Miller, F. W. J. Olver, and J. H. Wilkinson (National Physical Laboratory), *Modern Computing Methods*, *Notes on Applied Science*, 2nd ed. (H. M. Stationary Office, London, 1961), Vol. 16.
[56] A. van Wijngaarden, in *Cursus: Wetenschappelijk Rekenen B*, *Process Analyse* (Stichting Mathematisch Centrum, Amsterdam, 1965), pp. 51–60.
[57] E. J. Weniger, Comput. Phys. Rep. **10**, 189 (1989).
[58] A. V. Manohar and I. W. Stewart, Phys. Rev. Lett. **85**, 2248 (2000).
[59] The numerical value of $A_{60}=-30.924\,15(1)$ has been obtained by K. Pachucki after the reevaluation of certain poorly convergent one-dimensional numerical integrals in his calculation [15].
[60] K. Pachucki, J. Phys. B **32**, 137 (1999).
[61] A. N. Artemyev, V. M. Shabaev, and V. A. Yerokhin, Phys. Rev. A **52**, 1884 (1995).
[62] A. N. Artemyev, V. M. Shabaev, and V. A. Yerokhin, J. Phys. B **28**, 5201 (1995).
[63] V. M. Shabaev, A. N. Artemyev, T. Beier, and G. Soff, J. Phys. B **31**, L337 (1998).
[64] V. M. Shabaev, A. N. Artemyev, T. Beier, G. Plunien, V. A. Yerokhin, and G. Soff, Phys. Rev. A **57**, 4235 (1998).
[65] K. Pachucki and H. Grotch, Phys. Rev. A **51**, 1854 (1995).
[66] A. S. Yelkhovsky, Zh. Éksp. Teor. Fiz. **86**, 865 (1998) [JETP **86**, 472 (1998)].
[67] T. Beier and G. Soff, Z. Phys. D: At., Mol. Clusters **8**, 129 (1988).
[68] S. M. Schneider, W. Greiner, and G. Soff, J. Phys. B **26**, L529 (1993).
[69] S. G. Karshenboim, Zh. Éksp. Teor. Fiz. 103, 1105 (1993) [JETP **76**, 541 (1993)].
[70] I. Goidenko, L. Labzowsky, A. Nefiodov, G. Plunien, and G. Soff, Phys. Rev. Lett. **83**, 2312 (1999).
[71] S. Mallampalli and J. Sapirstein, Phys. Rev. Lett. **80**, 5297 (1998).
[72] V. A. Yerokhin, Phys. Rev. A **62**, 012508 (2000).